EUROPEAN ORGANIZATION FOR NUCLEAR RESEARCH

CERN-PPE/91-127
11.7.1991

GROUND STATE PROPERTIES OF NEUTRON-DEFICIENT PLATINUM ISOTOPES*

Th. Hilberath, St. Becker, G. Bollen, H.-J. Kluge, U. Krönert, G. Passler,
Institut für Physik, Universität Mainz, D-6500 Mainz, Fed. Rep. Germany

J. Rikovska,
Clarendon Laboratory, Parks Road, OX1 3PU, Oxford, U.K.

R. Wyss,
Joint Institute for Heavy Ion Research, ORNL, PO Box 2009, Oak Ridge, TN 37831, USA

and the ISOLDE Collaboration, PPE Div., CERN, Geneva, Switzerland

Dedicated to P. Armbruster on the occasion of his 60th birthday

Abstract. The hyperfine structure splitting and the isotope shift in the λ = 266 nm transition of Pt isotopes within the mass range $183 \leq A \leq 198$ have been determined by Resonance Ionization Mass Spectroscopy (RIMS) in combination with Pulsed-Laser Induced Desorption (PLID). The Pt isotopes were obtained at the on-line isotope separator ISOLDE-3/CERN as daughters of the primarily produced Hg isotopes. Magnetic moments, quadrupole moments, and changes in the mean-square charge radii are deduced and compared with results of a particle-triaxial rotor model and mean field calculations. Good agreement with experimental data (including nuclear level schemes and transition probabilities) can only be obtained if triaxial shape is admitted. The calculations yield a smooth transition in the shape of odd-A Pt nuclei from a slightly deformed, nearly oblate ^{195}Pt via triaxial $^{193-187}$Pt to a strongly deformed nearly prolate ^{177}Pt.

Submitted to Z. Phys. A

IS150)

*) This publication comprises part of the thesis of Th. Hilberath

1. Introduction

During the last two decades great effort has been made to determine the nuclear ground state properties of long isotopic chains in the region of transitional nuclei near the proton shell closure at Z = 82. Hyperfine structure and isotope shift and hence nuclear spins, moments and changes in the mean-squared nuclear charge radii are known for mercury [1-7] in the mass range $181 \leq A \leq 206$, in case of gold [8-11] for $183 \leq A \leq 199$, and now for platinum [12-14] in the isotopic series $183 \leq A \leq 198$.

A surprising result was obtained in 1972: Between ^{185}Hg and ^{187}Hg a sudden drastic change in the isotope shift (IS) and hence in the mean-squared nuclear charge radius was observed [1] which was explained as due to the near degeneracy of nuclear states of different shape.

This discovery offered the key for understanding the complicated rotational band structure observed in the neighbouring even-even Hg nuclei by γ-spectroscopy as due to shape coexistence [15]. Later on, a drastic odd-even staggering of the nuclear shape was found in the very light Hg isotopes [4,7] and, in case of ^{185}Hg [6], shape coexistence was observed to be manifested in a strongly deformed ground state (I = 1/2) and a slightly deformed isomeric state (I = 13/2).

Subsequently systematic studies were also performed in the neighbouring gold isotopic chain. A break in the IS similar to that observed in Hg was also found in Au between ^{187}Au and ^{186}Au, i.e. one neutron number earlier than in Hg. No shape staggering was observed: The Au nuclei below ^{186}Au remain strongly prolate-deformed in their ground states due to the polarization-driving effect of the $\pi h_{9/2}$ intruder configuration.

In this publication, we report on laser spectroscopy experiments in the platinum isotopic chain for $183 \leq A \leq 198$. Resonance Ionization Mass Spectroscopy (RIMS) was applied in combination with Pulsed Laser Induced Desorption (PLID) in order to achieve high sensitivity and a good signal-to-background ratio [14,16]. Similar experiments have been reported by an Orsay-Montreal Collaboration [13,17].

After a brief description of the RIMS–PLID technique (Section 2) we present our results on moments and changes in charge radii and use all IS data available for a multi-dimensional King plot analysis of the changes in the nuclear charge radius. Finally, deformation parameters $\langle\beta^2\rangle^{1/2}$ are deduced from this data set by use of the Droplet Model (Section 3).

Section 4 presents a brief description of the Lund particle-triaxial rotor model [18] and its detailed application to Pt isotopes. Although the full calculation takes into account not only the present results but also data from numerous nuclear spectroscopy and nuclear orientation studies, only ground state electromagnetic moments are discussed in this paper (for full calculation and list of references see [19]).

In Section 5 we describe mean field calculations based on the Strutinsky shell correction approach [20-22]. For odd-A Pt nuclei ($175 \leq A \leq 193$) this calculation has been performed for the first time.

In Section 6 we discuss implications of the two independent model calculations and the experimental data presented in this paper on the shape evolution of the ground states of odd-A Pt nuclei.

2. Experimental procedure and performance

In the following we briefly describe the method used for the investigation of neutron-deficient platinum isotopes. Experimental details have recently been published elsewhere [16]. Figure 1 shows the experimental setup which was installed at the on-line isotope separator ISOLDE-3 at CERN/Geneva. Since no target-ion source system is available for direct production of platinum isotopes, the nuclei were obtained as daughters in the decay of isobaric Hg isotopes. Mercury nuclei were produced by a spallation reaction with 600 MeV protons from a molten lead target.

After ionization and mass separation the Hg ion beam was focused onto a target wheel made of graphite (Fig. 1). When the selected isotope had decayed via Au into Pt, this wheel was turned by 180^0 and the implanted atoms were evaporated by means of PLID [16] using 10 ns light pulses (λ = 532 nm) of a Nd:YAG laser. The atoms desorbed as a short pulse were step-wise resonantly excited and finally ionized by the light pulses of two dye lasers (λ_1 = 266 nm, λ_2 = 452 nm) and by the frequency-doubled output of a second Nd:YAG laser (λ_3 = 532 nm) used also for pumping the dye lasers. The laser pulses were fired with a delay of 10 μs in respect to the desorption laser pulse in order to obtain maximum temporal overlap of the pulsed thermal atomic beam with the laser beams for resonance ionization. The ions created in resonance were detected mass selectively by means of a time-of-flight (TOF) spectrometer, a 40^0 ion reflector and a microchannel plate detector. This TOF spectrometer and several pulsed electrodes and deflectors served for reduction of background ions due to the desorption process and non-resonant ionization [16].

The overall detection efficiency ε_{exp} of the RIMS apparatus (which is defined as the ratio of the number of photo ions detected in resonance to the number of atoms implanted into the target) was determined in the on-line run to be of the order of $\varepsilon_{exp} = 5 \cdot 10^{-7}$ for platinum [16]. A background counting rate of typically one event per 1000 laser pulses was observed in the on-line experiments.

3. Data evaluation

The quantities measured by means of the RIMS/PLID method are the hyperfine structure splitting (HFS) and the IS in the first excitation step (Fig. 2) leading from the $5d^96s\ ^3D_3$ ground state to the excited $5d^96p$ state (J = 4). As an example the ion signals of ^{191}Pt and ^{183}Pt are shown in Fig. 3. In case of short-lived ^{183}Pt the measured HFS spectrum was corrected for nuclear decay during the scan of the laser wavelength. The frequency scale was calibrated using the simultanously recorded absorption spectrum of molecular iodine. A Gaussian was fitted to each optical resonance in the RIMS signals of the radioactive isotope. The superfluorescent laser background was taken into account by an additional Gaussian with a width of typically $\Delta\nu$(FWHM) = 10 GHz. Hence, the fitting parameters were a common center and the widths and the heights of the two Gaussians. In case of even–A Pt isotopes, the single resonance observed immediately yields the IS.

In case of odd-A Pt isotopes, the HFS pattern was fitted by A- and B-factors of the ground state and the B-factor of the excited 6p-state and the well known formula for the HFS splitting

$$E_{HFS}(F) = E_{FS}(J) + \frac{C}{2} \cdot A + \frac{3/4C(C+1) - I(I+1)J(J+1)}{2I(2I-1)2J(2J-1)} \cdot B \qquad (1)$$

with

$$C = F(F+1) - I(I+1) - J(J+1) , \qquad (2)$$

$$A = \frac{\mu_I \langle JJ | H(0) | JJ \rangle}{IJ} \qquad (3)$$

and

$$B = e\, Q_s \langle JJ | \varphi_{zz}(0) | JJ \rangle . \qquad (4)$$

The ratio of the A-factors of the ground and the excited 6p-state was fixed to the value of the isotope ^{195}Pt by

$$\frac{A(5d^9 6s\ ^3D_3,\ ^{195}Pt)}{A(5d^9 6p\ 7_4,\ ^{195}Pt)} = 3.78(1) , \qquad (5)$$

where the unknown HFS splitting of the 6p-state was determined with the help of a reference atomic beam apparatus to be

$$A(5d^9 6p\ 7_4, ^{195}Pt) = 1.508(5)\ GHz . \qquad (6)$$

The sign of the A-factor of the ground state of the I = 1/2 isotopes ^{185m}Pt and ^{183}Pt was determined from the intensity ratio of the two HFS components. In case of ^{183}Pt, for example, the experimental intensity ratio of the two components (Fig. 2) is V_{exp}= 1.4(5). Theoretically one obtains $V_{theo}(A > 0)$ = 1.3 and $V_{theo}(A < 0)$ = 0.77. Hence, the A-factor (and by this the magnetic moment μ_I) is positive with high probability.
The experimental isotope shifts are compiled in Table 1 and compared with results of Duong et al. [13]. The agreement is very good. In case of ^{185}Pt, Duong et al. determined the I = 9/2 ground state, while the isomer ^{185m}Pt (I = 1/2) was investigated in the present work.
The A-factor of the ground state and the B-factors of the ground state and excited state are compiled in Table 2. The only stable Pt nucleus with I ≠ 0, namely ^{195}Pt (I = 1/2), was chosen as reference isotope for the determination of the magnetic moments of the unstable isotopes. From the precisely known values [23,24] of the magnetic moment and the A-factor of the ^{195}Pt ground state (g.s.) one calculates

$$\mu_I\ (^xPt) = 0.214(2) \cdot A_{g.s.}(^xPt) \cdot I(^xPt) \qquad (7)$$

where the error assignment of 1 % accounts for the uncertainty of the hyperfine anomaly. The magnetic moments are compiled in Table 3 and compared to independently determined values [13,25-27].
The B-factor of the $^3D_3$-ground state is related to the spectroscopic quadrupole moment by (see Appendix 1)

$$Q_s = -0.685\ b/GHz \cdot B(^3D_3) \qquad (8)$$

The results are compiled in Table 4 and compared with the data of other measurements by laser spectroscopy [13] and nuclear orientation [25,26].
The spectroscopic quadrupole moment has to be corrected for core polarization by

$$Q_s^{corr} = Q_s \; / \; (1 - R) \qquad (9)$$

with a Sternheimer shielding factor R. An antishielding of $R_{5d} = -0.3(1)$ is estimated by R.M. Sternheimer [28] based on a calculation for praseodynium [29] and an estimate of R_{5d} for rare earth elements [30,31]. At the same time Sternheimer points to a systematic investigation by Childs and Cheng [32] of R as a function of filling the 5d-shell. A value of $R_{5d}(Pt, {}^3D_3) = -0.1$ is obtained from these systematics. This value is used in Table 4 for correcting the spectroscopic quadrupole moments.
The data compiled in Tables 3 and 4 are generally in good agreement except for some minor inconsistencies in case of ^{189}Pt. Note that the data of Duong et al. were taken from Table 1 of Ref. [13].
The experimental isotope shift $\delta\nu_i^{A,A'}$ between two isotopes with mass number A and A' in an optical transition i of frequency ν_i is the sum of the nuclear volume effect ($\delta\nu_{field}^{A,A'}$) and the mass shift ($\delta\nu_{mass}^{A,A'}$) given by [33]

$$\delta\nu_i^{A,A'} = \nu_i^{A'} - \nu_i^{A} = \delta\nu_{field}^{A,A'} + \delta\nu_{mass}^{A,A'} \qquad (10)$$

The mass shift is the sum of the normal mass shift (NMS) and the specific mass shift. The NMS is given by [33]

$$\delta\nu_{NMS}^{A,A'} = \frac{\nu_i^{A,A'}}{1836} \; \frac{A' - A}{AA'} \quad , A' > A \quad . \qquad (11a)$$

For the transition $5d^9 6s \, {}^3D_3$ to $5d^9 6p \; 7_4$ (λ = 266 nm) in Pt, the usual estimate of the SMS in s --> p transitions can be used [33]

$$\delta\nu_{SMS}^{A,A'} = (0.3 \pm 0.9) \; \delta\nu_{NMS}^{A,A'} \quad . \qquad (11b)$$

The contribution of the mass shift to the isotope shift is small in case of heavy elements like Pt and ranges between $\delta\nu_{mass}^{194,195} = -21(15)$ MHz and $\delta\nu_{mass}^{194,183} = 247(171)$ MHz.

The field shift is connected by [33]

$$\delta\nu_{field}^{A,A'} = F_i \cdot \lambda^{A,A'} \qquad (12)$$

to the nuclear radius parameter

$$\lambda^{A,A'} = \delta\langle r^2 \rangle^{A,A'} + \frac{C_2}{C_1} \delta\langle r^4 \rangle^{A,A'} + \frac{C_3}{C_1} \delta\langle r^6 \rangle^{A,A'} \qquad (13)$$

with tabulated coefficients C_j [34] and the electronic factor F_i. In order to be consistent with the data treatment in case of mercury [7] and gold [9-11], we use the multi-configuration Dirac-Fock value by Fricke [35] for the λ = 266 nm transition

$$F_{266} = -20.78 \text{ GHz/fm}^2 \quad . \tag{14}$$

A discussion of this parameter is given in Appendix 2. The resulting λ-parameters and the changes in mean-squared charge radii are compiled in Table 1.

3.1 Multi-Dimensional King Plot Analysis

Isotope shifts are now known in the λ = 266 nm transition for both the stable and neutron-deficient isotopes (this work and Ref. [12,13]) In addition, numerous IS investigations have been performed on stable isotopes in different optical transitions [36-40]. In order to base the following interpretation on an improved and consistent data set, a multi-dimensional King plot analysis [41] was performed. Good consistency was found, indicated by a reduced χ^2 = 0.85. The results are given in Table 5. As can be seen from a comparison with Table 1, the errors are reduced in all cases, where more than one measurement was performed.

3.2 Determination of deformation parameters

It should be noted that the data of Tables 1 to 5 are nuclear model independent. In the following, the Droplet model [42] will be used to extract information on the model-dependent quadrupole deformation parameter $\langle\beta_2^2\rangle$ from the measured isotope shifts. The procedure is described by Ahmad et al. [43]: The change in the mean-square charge radii can be decomposed into one contribution accounting for the change in nuclear volume (at constant deformation) and a second describing the change in deformation (at constant nuclear volume)

$$\delta\langle r^2\rangle_{exp}^{A,A'} = \delta\langle r^2\rangle_{sph}^{A,A'} + \delta\langle r^2\rangle_{def}^{A,A'} \tag{15}$$

Corrections due to higher radial moments ($\langle r^4\rangle$, $\langle r^6\rangle$, ...) are taken into account [43]. The spherical part of (15) is calculated with the help of the Droplet model [42], i. e. $\delta\langle r^2\rangle_{sph} = \delta\langle r^2\rangle_{Droplet}$. Therefore, the experimentally determined changes in the mean-squared charge radii (Table 1 resp. Table 5) allow calculation of the change in $\langle r^2\rangle$ due to a change in deformation between the isotopes A and A' by

$$\delta\langle\beta_2^2\rangle^{A,A'} = \left[\frac{5}{4\pi}\overline{\langle r^2\rangle}_{Droplet}\right]^{-1} \cdot (\delta\langle r^2\rangle_{exp} - \delta\langle r^2\rangle_{Droplet}) \tag{16}$$

where only quadrupole deformation β_2 is considered. The values obtained from the data of the multi-dimensional King plot analysis are given in Table 6.
If triaxial shape is included, the $\langle r^2\rangle$ value is given by [44,45]

$$\langle r^2\rangle = \langle r^2\rangle_{Droplet} + \frac{5}{4\pi}\langle r^2\rangle_{Droplet}\left\{\langle\beta_2^2\rangle + \frac{3}{10}\langle\beta_2^3\rangle \cos\gamma(1 - 4\sin^2\gamma)\right\} \tag{17}$$

with the asymmetry parameter γ. For $\gamma = 30^0$, the $\langle\beta_2^3\rangle$ contribution disappears

and eq. (17) reduces to the corresponding equation for axially symmetric nuclei. For $\beta_2 = 0.2$, the $\langle\beta_2^3\rangle$ term contributes only 6 % to the deformation part of eq. (17) dominated by $\langle\beta_2^2\rangle$. This shows that the isotope shift is very insensitive to triaxial shape. As a consequence, the triaxial degree of freedom is usually neglected in the analysis of isotope shifts.
Absolute deformation parameters $\langle\beta_2^2\rangle^{1/2}$ can be obtained via the relation

$$\langle\beta_2^2\rangle^A = \langle\beta_2^2\rangle^{A'} + \delta\langle\beta_2^2\rangle^{A,A'} \qquad (18)$$

by use of the precisely known B(E2, $2^+ \rightarrow 0^+$) value of ^{194}Pt [46]. The results derived from the IS's are given in column 3 of Table 6. They are compared with B(E2) values known for the even-A Pt isotopes [47]. The agreement is very good. If the Droplet parametrization of Berdichevsky and Tondeur [48] is used instead of that of Myers and Schmidt [42], the resulting deformation parameters $\langle\beta_2^2\rangle$ are about 10 % lower (larger) for A > 194 (A < 194) than given in Table 6. There is a tendency that the parametrization of Berdichevsky and Tondeur is slightly better (see also Ref. [49]).
Nevertheless we use the results of the Droplet model of Myers and Schmidt in order to be consistent with the procedure applied in case of Hg [7] and Au [10,11].
The last column of Table 6 shows the deformation parameters calculated from the spectroscopic quadrupole moments under the assumption of strong coupling of the valence neutron by

$$Q_s = \frac{I(2I-1)}{(I+1)(2I+3)}\, Q_0 \qquad (19)$$

and

$$Q_0 = \frac{3}{\sqrt{5\pi}}\, Z\, R_0^2 \langle\beta_2\rangle \left(1 + \frac{2}{7}\sqrt{\frac{5}{\pi}}\,\langle\beta_2\rangle\right) \quad . \qquad (20)$$

Assuming axially symmetric nuclei the deformation parameters calculated from the IS and from the spectroscopic quadrupole moments agree very well. Detailed theoretical investigation leads instead to triaxial ground state shapes for most of the Pt-isotopes as will be discussed in the following sections.
The changes in charge radii and the deformation parameters calculated from the IS under assumption of axial symmetry are shown in Fig. 4 and 5 for platinum, gold and mercury.

4. Particle-triaxial rotor calculation.

The model has been described in detail in several papers [see e.g. 18,50,51]. The single-particle Hamiltonian used has the form [50]

$$H_{s.p.} = H_{h.o.}(\varepsilon_2, \gamma) - \kappa(N)\hbar\omega_0 \{2\vec{l}\cdot\vec{s} + \mu(N)(l^2 - \langle l^2\rangle_N)\} \qquad (21)$$

where H is the deformed harmonic oscillator Hamiltonian, and all the other symbols in (21) have their usual meaning. Diagonalization of the Hamiltonian (21) in the $|N l j \Omega\rangle$ basis and inclusion of pairing effects gives adiabatic quasi-particle energies and wavefunctions written as

$$\chi_\nu = \sum_{NIj\Omega} c^{(\nu)}_{NIj\Omega}\ \Phi_{NIj\Omega} \tag{22}$$

and their conjugate states

$$\tilde{\chi}_\nu = \sum_{NIj\Omega} (-1)^{j-\Omega}\ c^{(\nu)}_{NIj\Omega}\ \Phi_{NIj-\Omega} \tag{23}$$

where ν is the sequential number of a wavefunction χ_ν.

The core Hamiltonian is defined as

$$H_{core} = \sum (\hbar^2/2\Theta_i)(\vec{I}_i - \vec{j}_i)^2 \qquad ;\ i = 1,2,3 \text{ for } x,y,z \tag{24}$$

where $\vec{I}$ is the total nuclear spin and $\vec{j}$ is the spin of the odd particle. Θ_i is the hydrodynamical moment of inertia calculated from

$$\Theta_i = 4\ B\ \varepsilon_2^2\ \sin^2(\gamma + 2i\pi/3) \tag{25}$$

using Grodzin's empirical relation

$$\hbar^2/B = 1000/A^{7/3}\ (\text{MeV}). \tag{26}$$

H_{core} is exactly diagonalized in the strong-coupling basis

$$\Psi^{I(\nu)}_{MK} = [(2I+1)/16\pi^2]^{1/2} \sum_{NIj\Omega} c^{(\nu)}_{NIj\Omega} \left\{ D^I_{MK}\ \Phi_{NIj\Omega} + (-1)^{I-j}\ D^I_{M-K}\ \Phi_{NIj-\Omega} \right\} \tag{27}$$

yielding energy levels and total wavefunctions

$$\Phi^{I(\nu)}_M = \sum_{K,\nu} a^{I(\nu)}_K\ \Psi^{I(\nu)}_{MK}. \tag{28}$$

In all cases five single-particle orbitals above the Fermi level and five below were included into the diagonalization. The positive and negative parity systems were treated separately.

This choice of Hamiltonian implies that the core is approximated as a body of fixed shape, in principle not including vibrations or effects like γ-softness etc. Nevertheless, Larsson et al. [18] pointed out that there is some shape vibration amplitude present in the model within uncertainities of the core quadrupole components Q_{20} and Q_{22}, which can contribute a sizeable fraction of the total deformation in transitional nuclei.

Our calculation is dependent on up to five free parameters [19] which were changed from isotope to isotope. However, well-defined constraints on almost all of the free parameters exist which must be satisfied to ensure the fitted parameters have a physical meaning.

As can be seen in Table 8, there is full experimental information about the value of quadrupole deformation β_2 as extracted from both B(E2) values and ground

and isomeric state mean-square charge radii. However, one should take these values with caution as they have been extracted from experiment assuming rigid axially symmetrical nuclei. Furthermore, there is no exact analytical relation between ε_2 and β_2 for non-axially symmetrical shapes, and we can only estimate $\varepsilon_2 \approx 0.85 - 0.95\ \beta_2$ at deformations around 0.2 [52]. Despite these uncertainties, data shown in Table 8 serve as a useful guide to the dependence of deformation upon neutron number.

On the other hand, there is very little guidance concerning γ-deformation and this parameter is not open to direct measurement. The only data available is signature splitting in rotational bands, but this may not be directly relevant to the shape of the nuclear ground state. Theoretical calculation of Pt deformation parameters including γ have been made for even-even nuclei [53-58 and Refs. therein] and odd-A by Wyss [22].

Standard BCS procedure was used for calculating pairing parameters λ and Δ, with G_{n0} = 19.2 MeV and G_{n1} = 7.4 MeV [52]. λ_{BCS} and Δ_{BCS} were varied within a narrow interval around the calculated values (see ref. [19]). Deviation of λ_{fit} and Δ_{fit} from the BCS values led to improved fits for all isotopes except ^{183}Pt and ^{195}Pt. While the differences between λ_{fit} and λ_{BCS} were very small, deviations from BCS values were found for Δ_{fit} for neutron numbers $107 \leq N \leq 111$. The behaviour of Δ_{fit} can be understood as caused by the existence of a subshell closure at N = 108. This closure has been identified before in Pt isotopes [53,59] and its effect on the pairing energy discussed theoretically. We have investigated the single-particle level spectrum in the γ-plane ($0^0 \leq \gamma \leq 60^0$) for $0.15 \leq \varepsilon_2 \leq 0.25$ and the presence of the subshell gap at N = 108 is clearly seen.

It is well known that agreement between particle-rotor calculations and experiment is generally improved if a Coriolis attenuation parameter is introduced. There are two ways of doing this, (i) using a factor ξ, multiplying all single-particle matrix elements [18] and/or (ii) using a factor of the form $(u_1v_1 + u_2v_2)^\eta$ to be attached to each single-particle matrix element [60]. In our calculation of negative parity states the Coriolis attenuation factors ξ and η were not required ($\xi = \eta = 1.0$) apart from ^{177}Pt (see ref. [19]). An attenuation of up to 30 % [19] was needed in the calculation of positive parity bands based on a high-j $i_{13/2}$-orbital ($\xi > 0.7$, $\eta = 1$). Coriolis attenuations of this magnitude are commonly used in particle rotor calculations.

There are three more parameters of the model which were set and kept constant for most of the nuclei. These are the strengths of the $\vec{l}\cdot\vec{s}$ and l^2 terms in the modified oscillator potential, i.e. $\varkappa$ and μ, and the constant B in expression (26) for the moment of inertia.

Parameters $\varkappa$ and μ are generally dependent on the main oscillator quantum number N. We initially took $\varkappa$ = 0.062 (both N = 5 and 6) and μ = 0.43 (N = 5) and μ = 0.34 (N=6) following Bengtsson and Ragnarsson [56] in their calculation of high spin states in the rare earth region. However, we found that a better overall fit was achieved for $\varkappa$ = 0.0636 (N = 5 and 6), μ = 0.40 (N = 5, A = 177-185, and N = 6, all A) and μ = 0.39 (N = 5, A = 187-193). This choice changed the relative energies of the negative parity spherical $f_{7/2}$, $p_{3/2}$, $f_{5/2}$ and $p_{1/2}$ states and the positive parity $i_{13/2}$ state. We note that Nilsson et al. [52] used neutron parameters $\varkappa$ = 0.0636 and μ = 0.393 in the mass region around A = 187 while $\varkappa$ = 0.062 and μ = 0.40 were adopted by Bacelar et al. [61] for

N = 6 neutron states in their calculation of ^{167,169} Yb; both these sets are well in line with those used here. The constant B has been calculated from Grodzin's formula (26).

Finally we note that we did not use any of the other options included in the present model — namely, using a variable moment of inertia or taking the $E_{2^+(1)}$ and $E_{2^+(2)}$ experimental energies as input data for calculation of moment of inertia. Also, we treated the recoil term in the Hamiltonian (24) as a one-body operator. The calculation has been done for each nucleus starting from an axially symmetrical shape (prolate for $^{177-185}$Pt, oblate for $^{187-195}$Pt). The fit was then improved by varying the deformation parameter γ. For each nucleus the number of experimental data fitted was never less than twenty, including energy levels of both parities up to $I \leq 21/2$, and multipole branching and mixing ratios of inter- and intra-band electromagnetic transitions. Unless there was a clear basis in the physics, smooth variation of all parameters with neutron number was required. Full details of the calculation have been published elsewhere [19]. Here we show only results for deformation parameters of the ground states and corresponding magnetic dipole and electric quadrupole moments.

We illustrate in Fig. 6 the quality of the fit obtained using ^{187}Pt as an example. The magnetic (a) and quadrupole (b) moments of the lowest-lying $3/2^-$ state and its energy (c) are shown as a function of γ for three different values of the deformation parameter ε_2, 0.15 and 0.22, representing lower and upper limit and 0.169, the best fitted value. Clearly, a $3/2^-$ state becomes the ground state only for $\gamma \geq 30^0$. This limits the possible values of gamma to $30^0 \leq \gamma \leq 60^0$. The quadrupole moment calculation allows all values of γ with ε_2 between 0.16 - 0.21 . The magnetic moment restricts deformation parameters to $20^0 \leq \gamma \leq 40^0$ for $0.15 \leq \varepsilon_2 \leq 0.22$. The experimental limits on ε_2 yielded by the mean square radii is $0.15 \leq \varepsilon_2 \leq 0.19$ (using the relationship between ε_2 and β_2 given above and table 8). Overlap of all the conditions narrows the limits to $0.165 \leq \varepsilon_2 \leq 0.19$ and $30^0 \leq \gamma \leq 60^0$. The final values, quoted in Table 7 have been chosen from the best fit to the lowest excited states in ^{187}Pt (see [19]). We stress that *all* available experimental data had to be employed to choose the best overall fit values of deformation parameters.

5. Mean field total routhian surface (TRS) calculations

Mean field calculations based on the Strutinsky shell correction approach [20] have been performed for nuclei in the mass A=180 region [22]. The calculations employ a deformed Woods-Saxon potential with a universal set of parameters described in [21]. The macroscopic part of the energy is determined by the liquid drop energy, E_{ld}, which in the present calculations is taken from ref. [62]. The microscopic contribution to the energy, δE_{shell}, derives from the shell effect. The total energy of the nucleus, $E(Z, N, \hat{\beta})$, is obtained as

$$E(Z, N, \hat{\beta}) = E_{ld}(Z, N, \hat{\beta}) + \sum e^i_{sp} - E_{Strut}(Z, N, \hat{\beta}) =$$

$$= E_{ld}(Z, N, \hat{\beta}) + \delta E_{shell}(Z, N, \hat{\beta}) \qquad (29)$$

where $\hat{\beta} = \beta_2, \beta_4$ and γ and e^i_{sp} are the single particle energies given by the

Woods-Saxon potential. The calculations are performed on a rectangular grid where the total energy is minimized at each gridpoint with respect to the hexadecapole deformation parameter β_4. The β_4 parameterization of the nuclear potential is described in more detail in ref. [21]. In the present calculation, the deformation points on the grid are chosen as

$$\beta_2 \cos(\gamma + 30^\circ) = 0.05(0.05)0.40 \tag{30a}$$

$$\beta_2 \sin(\gamma + 30^\circ) = -0.20(0.05)0.30 \tag{30b}$$

and

$$\beta_4 = -0.08(0.04)0.04 + Id \tag{30c}$$

where *Id* stands for the β_4-value which minimizes the liquid drop energy at each chosen γ and β_2 and the values in parenthesis give the steplength between each calculated point.

The residual particle-particle interaction is approximated with a monopole pairing force using the BCS approach. At each deformation point, the BCS equations are solved self-consistently and the pairing energy δE_{pair} is added to the total energy.

Early calculations of Potential Energy surfaces (PES) of even-even nuclei in this mass region have successfully described the prolate/oblate energy difference in Hg and Pt nuclei (see ref. [63]). The present calculations are extended to include odd proton and neutron numbers and different quasi-particle configurations. The calculations also treat the change of the nuclear shape as a function of the rotational frequency $\hbar\omega$. This is accomplished by adding the cranking term $-\omega j_x$ to the Hamiltonian, resulting in a set of Total Routhian Surfaces (TRS) [22], where Routhian stands for the energy in the rotating frame (for more details see [64]). Each TRS has a specified parity and signature, but no other quantum numbers are preserved. Configurations are allowed to change adiabatically over a surface. This implies that at each γ and β_2 value, the energetically most favoured configuration is determined. However, this configuration will not be the same over the entire surface. Since the present work is focused on ground state properties of the Pt isotopes, only the TRS of the lowest calculated frequency is considered, that is for $\hbar\omega$ = 0.05 MeV. At this frequency, the cranking term in the Hamiltonian is very small and the TRS becomes essentially identical to the PES.

Selected results from the TRS calculations are given in Table 7. Fig. 7 displays the shape evolution of odd Pt-isotopes with negative parity and signature α = -1/2 as a function of neutron number N. The signature is determined as I = α *mod* 2, i.e. α = -1/2 corresponds to a spin sequence of I = 3/2, 7/2, 11/2 etc. The TR surfaces of positive parity correspond to the occupation of the $i_{13/2}$ neutron unique parity orbital. The calculated deformations of the $i_{13/2}$ orbital follow a similar shape change from prolate to oblate as the negative parity orbitals, although differences are present due to different polarization properties. In the TRS calculations the deformation of each configuration is a dynamical variable which is changing with spin. The $i_{13/2}$ configuration in ^{185}Pt, which is the ground state, is calculated to be essentially prolate, but to become more

triaxial with increasing spin. We have chosen to display the energy surfaces of the negative parity states, since they form the ground state for most of the odd Pt isotopes.

6. Discussion

Previous theoretical investigations have mainly concerned even-even neutron-deficient Pt nuclei. Potential energy surfaces (PES) calculations [54,55,58,63] have predicted a complex shape development from light prolate (with ^{176}Pt close to triaxial) to heavier oblate via γ-soft nuclei around N = 108. Experimental ground state band E_4^+/E_2^+ energy ratios in $^{178-194}$Pt are mostly close to 2.5 (see Table 8) indicating a γ-soft shape for the ground state of these nuclei. Also, the moment of inertia dependence on $(\hbar\omega)^2$ of the ground state band shows deviations from a straight line even at lowest frequencies, pointing again towards γ-softness and shape coexistence [65-67]. The main question then arises - what will be the shape of an odd-A nucleus, where the odd neutron is coupled to a γ-soft core?

There have been attempts to use the particle-rotor model for some of the nuclei of interest (negative parity states in $^{185-187}$Pt [68,69], $^{187-191}$Pt [13], positive and negative parity states in ^{187}Pt [70], positive parity in $^{189-193}$Pt [71,72] and negative parity states in ^{195}Pt [73,74]). Apart from a successful calculation of the $i_{13/2}$ system in heavier Pt, showing clearly its non-axial character, other calculations were too limited in scope to offer general conclusions.

The present particle-triaxial rotor calculation has been performed consistently for the whole chain of $177 \leq A \leq 195$ Pt isotopes with the aim of following the development of model parameters as a function of neutron number. Parameters chosen to calculate ground and isomeric state electromagnetic moments were in addition required to fit excited energy levels and transition probabilities. In this way all relevant spectroscopic data were incorporated, assuring maximal internal consistency of the calculation.

Results of the calculation of electromagnetic moments are given in Table 9. Previous calculations by Duong et al. [13] and results for axially symmetrical shapes in the present calculation are shown for comparison. The present calculation yields in all cases magnetic moments with correct sign and magnitude, in contrast to the calculation by Duong et al. Turning to electric quadrupole moments we reproduce the change in sign (and magnitude) of the quadrupole moment of ^{185}Pt ground state as compared to $^{187-191}$Pt without invoking a sudden prolate-oblate [26,75] or prolate-triaxial [13,76] shape change.

The excellent agreement of the calculation with experiment shows in particular, that two deformation parameters ε_2 and γ are fully adequate to describe the shape evolution of the odd-A Pt ground states indicating a *gradual* transition between the oblate and prolate axial symmetries over a range of neutron number (see table 7). Table 8 shows that the calculated ε_2 reproduces very closely the quadrupole deformation values extracted from mean square charge radii.

Comparison of the first 2^+ state energies and the ground-state band E_4^+/E_2^+ ratios in the cores used in the present calculations and experimental data on even-even Pt nuclei (see Table 8) shows that, as a common feature, the calculated

cores are more deformed and show less evidence for γ-softness. It seems feasible to connect this phenomenon with a polarizing effect of the odd neutron, coupled to an otherwise very soft even-even nucleus. As a result, the core achieves a certain stable deformed shape, most likely dependent upon the particular odd-neutron orbital. This would imply shape coexistence for different single particle excitations within the same nucleus. The results of fitting positive and negative parity states in $^{185-195}$Pt [19] give evidence for such coexistence. From this point of view the change in sign of the quadrupole moment between A = 185 and A = 187 is simply a consequence of different configurations involved in ^{185}Pt ($I^{\pi} = 9/2^{+}$ of $i_{13/2}$ spherical origin) and ^{187}Pt ($I^{\pi} = 3/2^{-}$ consisting of components of $f_{5/2}$, $p_{3/2}$ and $p_{1/2}$ spherical parentage) ground states.

A similar conclusion was drawn by Ragnarsson and Semmes [51] for ^{185}Au (an odd proton coupled to even-even Pt core). Their total-energy-surface calculation gives clearly different minima for configurations of different spherical origin. However, the particle-triaxial rotor model in its present form cannot self-consistently include different configurations with individual deformations in one nucleus. Difficulties in such a calculation concern the absolute energy scale and the treatment of configuration mixing.

The results of the mean field calculation are shown in Fig. 7 and Table 7. This calculation, performed for odd-A Pt isotopes for the first time, shows several distinctive features. The two lightest isotopes $^{175-177}$Pt show a pronounced softness in β_2. The minimum at smaller deformation in $^{175-177}$Pt also shows γ-softness. The shape coexistence of the light Pt nuclei has been discussed in several papers [65,67,77]. The main difference between the two shapes is believed to be related to the occupation of the $\pi h_{9/2}$ intruder configuration. The Pt isotopes with $101 \leq N \leq 105$ show prolate shapes with large deformation, implying that the $h_{9/2}$ proton orbital is almost fully occupied. With increasing neutron number, the neutrons favour less deformed shapes and at N = 107 (^{185}Pt) the nuclear shape starts to develop γ-softness, which is increasing with N. We calculate a predominantly prolate (although triaxial) shape and a coexisting minimum at oblate shape for ^{187}Pt (Fig. 7). A mixing between the oblate and triaxial configurations which is beyond the present model and which is expected to occur especially in a γ-soft nucleus, may lead to a different effective shape and γ. In ^{189}Pt the calculation predicts a completely γ-unstable shape, which develops into more stable triaxial deformation in ^{191}Pt and almost oblate shape in ^{193}Pt (see Fig.7).

Experimentally, the measured quadrupole moments of $^{187-191}$Pt ground states are negative. It has been shown in the particle-triaxial rotor model calculation that a mixing of different quasi-particle configurations at triaxial shape can produce a negative quadrupole moment (see [19] and Fig. 6). Certain configurations have a negative spectroscopic quadrupole moment even at prolate shapes. Therefore calculated shapes in the mean field model for $^{187-191}$Pt do not disagree with experiment. In addition, the single particle levels are not accurate to more than a few hundred keV and minor changes will effect the oblate/prolate energy difference.

It follows from the above that in the present mean field approach it is difficult to predict the exact neutron number at which the change to negative quadrupole moments occurs, although the general trend from prolate to triaxial-oblate is nicely reproduced. We stress that both models yield a smooth change in γ with

N and no sudden shifts in γ are predicted. It is interesting to compare deformation parameters from TRS calculation and from particle-triaxial rotor model. As is shown in Table 7, parameters β_2, corresponding to the TRS lowest minimum, show a striking agreement with β_2 extracted from mean-square charge radii and ε_2 fitted in the particle-triaxial rotor calculations. The parameter γ shows similar development in the heavier isotopes in both models, but there is some discrepancy below ^{185}Pt.

There might be several reasons for this disagreement. In the particle rotor model, the extracted γ value for lower N isotopes is based on a detailed analysis of properties of the ground state bands and the relative positions of excited band heads. As shown in [19], the sensitivity of these observables to γ is rather limited in this region, in the absence of the ground state electromagnetic moments. Furthermore, in the TRS calculations, the γ-value is a dynamical variable, which is changing with spin and different for different quasi-particle configurations. In the particle-triaxial rotor calculation, the γ-value represents an average value obtained from a fit to all observed energy levels close to Fermi surface and their electromagnetic properties. A possible mixing of coexisting shapes (for example in ^{177}Pt) cannot be described either in the mean field or the particle-triaxial rotor model. Another difference between the two calculations origins from the hexadecapole degree of freedom, which has not been used in the particle-triaxial rotor model. It would be interesting to investigate the influence of the ε_4 parameter, using the values predicted by the TRS calculations. It would also be desirable for the lightest Pt isotopes to have experimental data on electromagnetic moments and mean square radii, which are predicted to drop significantly around N = 95 - 97.

7. Conclusions

Hyperfine structure splitting and isotope shifts have been determined for the Pt isotopes in the range $183 \leq A \leq 198$ by means of Resonance Ionization Mass Spectrometry (RIMS) in combination with Pulsed Laser Induced Desorption (PLID). Hence, on-line laser spectroscopy could be extended to refractory elements. Mean-square charge radii and the electromagnetic moments of the nuclear ground state are evaluated from the experimental data. Information on nuclear ground state properties is now available down to neutron number N = 101 for Hg, Au and Pt.

Two independent model calculations have been performed to interpret ground state properties of odd-A Pt isotopes. Both calculations predict a very *gradual* change in shape over a wide range of neutron number, through over a variety of triaxial shapes in sharp contrast to previous suggestions of a sudden prolate-oblate shape change between ^{185}Pt and ^{187}Pt. The situation in Pt is very different from the Hg isotopes, where the presence of the large Z = 80 gap at oblate shape favours distinct oblate configurations. The lack of any specific shell structure at Z = 78 in the Pt isotopes for oblate deformation may be the reason for the gradual shape development.

REFERENCES

[1] J. Bonn, G. Huber, H.-J. Kluge, L. Kugler, E. Otten, *Phys. Lett.* **38B**, 308 (1972)

[2] J. Bonn, G. Huber, H.-J. Kluge and E. Otten, *Z. Phys.* **A 276**, 203 (1976)

[3] C. Duke, H. Fischer, H.-J. Kluge, H. Kremmling, T. Kühl and E. Otten, *Phys. Lett.* **60A**, 303 (1977)

[4] T. Kühl, P. Dabkiewicz, C. Duke, H. Fischer, H. Kluge, H. Kremmling and E. Otten, *Phys. Rev. Lett.* **39**, 180 (1977)

[5] P. Dabkiewicz, F. Buchinger, H. Fischer, H.-J. Kluge, H. Kremmling, T. Kühl, A. C. Müller and H. A. Schuessler, *Phys. Lett.* **82B**, 199 (1979)

[6] H. Kremmling, P. Dabkiewicz, H. Fischer, H.-J. Kluge, T. Kühl and H. Schuessler, *Phys. Rev. Lett.* **43**, 1376 (1979)

[7] G. Ulm, S. K. Bhattacherjee, P. Dabkiewicz, G. Huber, H.-J. Kluge, T. Kühl, H. Lochmann, E. Otten, K. Wendt, S. Ahmad, W. Klempt, R. Neugart and the ISOLDE Collaboration, *Z. Phys.* **A325**, 247 (1986)

[8] J. Streib, H.-J. Kluge, H. Kremmling, R. B. Moore, H. Schaaf, K. Wallmeroth and the ISOLDE Collaboration, *Z. Phys.* **A321**, 537 (1985)

[9] K. Wallmeroth, G. Bollen, A. Dohn, P. Egelhof, J. Grüner, F. Lindenlauf, U. Krönert, J. Campos, A.R. Yunta, M. Borge, A. Venugopalan, J. Wood, R. B. Moore, H.-J. Kluge and the ISOLDE Collaboration, *Phys. Rev. Lett.* **58**, 1516 (1987)

[10] U. Krönert, S. Becker, G. Bollen, M. Gerber, T. Hilberath, H.-J. Kluge, G. Passler and the ISOLDE Collaboration, *Z. Phys.* **A331**, 521 (1988)

[11] K. Wallmeroth, G. Bollen, A. Dohn, P. Egelhof, U. Krönert, M. Borge, J. Campos, A. R. Yunta, K. Heyde, C. de Coster, J. Wood, H.-J. Kluge and the ISOLDE Collaboration, *Nucl. Phys.* **A493**, 224 (1989)

[12] J. Lee, G. Savard, J. Crawford, G. Thekkadath, H. Duong, J. Pinard, S. Liberman, F. Le Blanc, P. Kilcher, J. Obert, J. Oms, J. Putaux, B. Roussière and J. Sauvage, *Phys. Rev.* **C38**, 2985 (1988)

[13] H. T. Duong, J. Pinard, S. Liberman, G. Savard, J. K. P. Lee, J. E. Crawford, G. Thekkadath, F. L. Blanc, P. Kilcher, J. Obert, J. Oms, J. C. Putaux, B. Roussière, J. Sauvage and the ISOCELE Collaboration, *Phys. Lett.* **217B**, 401 (1989)

[14] T. Hilberath, S. Becker, G. Bollen, M. Gerber, H.-J. Kluge, U. Krönert, G. Passler and the ISOLDE Collaboration, *Z. Phys.* **A332**, 107 (1989)

[15] J. Hamilton, *Treatise on Heavy Ion Science* **8**, Nuclei far from Stability, Plenum Press, New York (1989)

[16] U. Krönert, S. Becker, G. Bollen, M. Gerber, T. Hilberath, H. Kluge and G. Passler, *Nucl. Instr. Meth.* **A300**, 522 (1991)

[17] J. Lee, G. Savard, J. Crawford, G. Thekkadath, H. Duong, J. Pinard, S. Liberman, F. Le Blanc, P. Kilcher, J. Obert, J. Oms, J. Putaux, B. Roussière, J. Sauvage and the ISOCELE Collaboration, *Nucl. Instr. Meth.* **B34**, 252 (1988)

[18] S. E. Larsson, G. Leander and I. Ragnarsson, *Nucl. Phys.* **A307**, 189 (1978)

[19] J. Rikovska, in *Exotic Nuclear Spectroscopy*, ed. Wm. C. McHarris, p. 139, Plenum Press, New York (1990)

[20] V. M. Strutinsky, *Nucl. Phys.* **A95**, 420 (1967)

[21] W. Nazarewicz, J. Dudek, R. Bengtsson, T. Bengtsson and I. Ragnarsson, *Nucl. Phys.* **A435**, 397 (1985)

[22] R.Wyss, W. Satuła, W. Nazarewicz and A. Johnson, *Nucl. Phys.* **A511**, 324 (1990)

[23] S. Büttgenbach, N. Glaeser, B. Roski, R. Träber, *Z. Phys.* **A317**, 237 (1984)

[24] C. Lederer and V. Shirley, *Table of Isotopes*, John Wiley and Sons, New York, 1978

[25] R. Eder, E. Hagn and E. Zech, *Phys. Lett.* **158B**, 371 (1985)

[26] R. Eder, C. J. Ashworth, I. Berkes, D. E. Brown, U. Dämmrich, I. S. Grant, A. G. Griffiths, E. Hagn, R. Hassani, P. Herzog, S. Ohya, M. Massaq, C. Richard-Serre, J. Rikovska, K. Schlösser, N. Severijns, N. J. Stone, W. Vanderpoorten, J. Vanhaverbeke, L. Vanneste, T. Wölfle, E. Zech and the ISOLDE Collaboration, *Hyp. Int.* **43**, 469 (1988)

[27] S. Ohya, K. Nishimura, N. Okabe and N. Mutsuro, *Hyp. Int.* **22**, 585 (1985)

[28] R. Sternheimer, *private communication* (1989)

[29] R. Sternheimer, *Phys. Rev.* **164**, 10 (1967)

[30] R. Sternheimer and R. Peierls, *Phys. Rev.* **A3**, 837 (1971)

[31] R. Sternheimer, Shielding and antishielding of nuclear quadrupole moments, *Z. Naturforsch.* **41**a, 24 (1986)

[32] W. Childs and K. Cheng, *Phys. Rev.* **A30**, 667 (1984)

[33] K. Heilig and A. Steudel, *At. Data Nucl. Data. Tab.* **14**, 613 (1974)

[34] E. Seltzer, *Phys. Rev.* **188**, 1916 (1969)

[35] B. Fricke, *private communication* (1989)

[36] V. Stacey and H. Kuhn, *Proc. Roy. Soc.* **A322**, 301 (1971)

[37] P. Baird and D. Stacey, *Proc. Roy. Soc.* **A341**, 399 (1974)

[38] G. Müller and R. Winkler, *Z. Phys.* **A273**, 313 (1975)

[39] W. Neu, G. Passler, G. Sawatzky, R. Winkler and H.-J. Kluge, *Z. Phys.* **D7**, 193 (1987)

[40] R.D. LaBelle, W. M. Fairbank Jr., R. Engleman Jr. and R. A. Keller, *J. Opt. Soc. Am.* **B6**, 137 (1989)

[41] C. Palmer, P. Baird, S. Blundell, J. Brandenberger, C. Foot, D. Stacey and G. Woodgate, *J. Phys.* **B17**, 2197 (1984)

[42] W. D. Myers and K.-H. Schmidt, *Nucl. Phys.* **A410**, 61 (1983)

[43] S. Ahmad, W. Klempt, C. Ekström, R. Neugart, K. Wendt and the ISOLDE Collaboration, *Z. Phys.* **A321**, 35 (1985)

[44] D. Grechukhin, *Sov. Phys.* JETP **11**, 1359 (1960)

[45] D. Grechukhin, *Sov. Phys.* JETP **13**, 261 (1961)

[46] S. Raman, C. Malarkey, W. Milner, C. Nestor jr. and P.H. Stelson, *Atomic Data and Nuclear Data Tables* **36**, 1 (1987)

[47] S. Raman, J. Nestor, S. Kahane and K. Bhatt, *Atomic Data and Nuclear Data Tables* **42**, 1 (1989)

[48] D. Berdichevsky and F. Tondeur, *Z. Phys.* **A322**, 141 (1985)

[49] S. Ahmad, W. Klempt, R. Neugart, E. Otten, P.-G. Reinhard, G. Ulm, K. Wendt and the ISOLDE Collaboration, *Nucl. Phys.* **A483**, 244 (1988)

[50] Ch. Vieu, S. E. Larsson, G. Leander, I. Ragnarson, W. de Wieclawik and J. S. Dionisio, *J. Phys.* **G4**, 531 (1978) and *Z. Phys.* **A290**, 301 (1979)

[51] I. Ragnarsson and P. B. Semmes, *Hyp. Int.* **43**, 425 (1988) and *private communication* 1989, 1990

[52] S. G. Nilsson, Chin Fu Tsang, A. Sobieczewski, Z. Szymanski, S. Wyech, Ch. Gustafson, I.-L. Lamm, P. Möller and B. Nilsson, *Nucl. Phys.* **A131**, 1 (1969)

[53] I. Ragnarson, A. Sobiczewski, R. K. Sheline, S. E. Larsson, B. Nerlo-Pomorska, *Nucl. Phys.* **A233**, 329 (1974).

[54] J. Sauvage-Letessier, P. Quentin and H. Flocard, *Nucl. Phys.* **A370**, 231 (1981)

[55] A. Ansari, *Phys. Rev.* **C33**, 321 (1986)

[56] T. Bengtsson and I. Ragnarsson, *Nucl. Phys.* **A436**, 14 (1987)

[57] A. Ansari, *Phys. Rev.* **C38**, 953 (1988)

[58] S. J. Krieger, P. Quentin, M. S. Weiss, J. Meyer, M. Meyer, N. Redon, H. Flocard and P. H. Heenen, *Nucl. Phys.* **A500**, 308 (1989)

[59] R. Bengtsson, P. Möller, J.R. Nix and Jing-ye Zhang, *Phys. Scr.* **29**, 402 (1984)

[60] F. S. Stephens, P. Kleinheinz, R. K. Sheline and R. S. Simon, *Nucl. Phys.* **A222**, 235 (1974)

[61] J. C. Bacelar, M. Diebel, C. Ellegaard, J. D. Garrett, G. B. Hagemann, R. Herskind, A. Holm, C.-X. Yang, J.-Y. Zhang, P. O. Tjom and J. C. Lisle, *Nucl. Phys.* **A442**, 509 (1985)

[62] W.D. Myers and W.J. Swiatecki, *Ann. Phys.* (N.Y.) **84**, 395 (1969)

[63] R. Bengtsson, T. Bengtsson, J. Dudek, G. Leander, W. Nazarewicz and J. ye Zhang, *Phys. Lett.* **183B**, 1 (1987)

[64] W. Nazarewicz, R. Wyss and A. Johnson, *Nucl. Phys.* **A503**, 285 (1989)

[65] G. D. Dracoulis, A. E. Stuchbery, A. P. Byrne, A. R. Poletti, S. J. Poletti, J. Gerl and R. A. Bark, *J. Phys.* **G12**, L97 (1986)

[66] M. J. A de Voigt, R. Kaczarowski, H. J. Riezebos, R. F. Noorman, J. C. Bacelar, M. A. Deleplanque, R. M. Diamond, F. S. Stephens, J. Sauvage, B. Roussière, *Nucl. Phys.* **A507**, 472 (1990)

[67] B. Cederwall, R. Wyss, A. Johnson, J. Nyberg, B. Fant, R. Chapman, D. Clarke, F. Khazaie, J.C. Lisle, J. N. Mo, J. Simpson and I. Thorslund, *Z. Phys.* **A337**, 283 (1990)

[68] B. Roussière, C. Bourgeois, P. Kilcher, J. Sauvage, M. Porquet and the ISOCELE Collaboration, *Nucl. Phys.* **A438**, 93 (1985)

[69] B. Roussière, C. Bourgeois, P. Kilcher, J. Sauvage, M. Porquet, A. Wojtasiewicz and the ISOCELE Collaboration, *Nucl. Phys.* **A485**, 111 (1988)

[70] B. Gnade, R. Fink and J. Wood, *Nucl. Phys.* **A406**, 29 (1983)

[71] S. K. Saha, M. Piiparinen, J. C. Cunnane, P. J. Daly, C. L. Dors, T. L. Khoo, F. M. Bernthal, *Phys. Rev.* **C15**, 94 (1977)

[72] T. L. Khoo, F. M. Bernthal, C. L. Dors, M. Piiparinen, S. K. Saha, P. J. Daly, J. Meyer-ter-Vehn, *Phys. Lett.* **60B**, 341 (1976)

[73] K. T. Hecht, G. R. Satchler, *Nucl. Phys.* **32**, 286 (1962)

[74] Y. Yamazaki, R. K. Sheline, *Phys. Rev.* **C21**, 531 (1976)

[75] R. Eder, I. Berkes, D. E. Brown, I. S. Grand, E. Hagn, P. Harding, R. Hassani, P. Herzog, B. Kastelein, A. Knipper, G. Marguier, M. Massaq, S. Ohya, H. Postma, J. Prinz, C. Richard-Serre, I. Romanski, K. Schlösser, N. J. Stone, W. Vanderpoorten, J. Vanhaverbeke, L. Vanneste, T. Wölfle, E. Zech and the ISOLDE Collaboration, *Hyp. Int.* **59**, 83 (1990)

[76] B. Roussière, F. Le Blanc, G. Savard, H. T. Duong, J. Pinard, S. Liberman, J. K. P. Lee, J. E. Crawford, G. Thekkadath, P. Kilcher, J. Obert, J. Oms, J. C. Putaux, J. Sauvage and the ISOCELE Collaboration, *Hyp. Int.* **43**, 473 (1988)

[77] J. L. Wood, *Proc. 4th Int. Conf. Nuclei Far From Stability, Helsingør, Denmark, June 1981*, ed. P.G. Hansen and O.B. Nielsen, CERN 81-09, p. 612

[78] H. Kopfermann, *Kernmomente*, Akademische Verlagsgesellschaft m.b.H., Frankfurt (1956)

[79] R. Engleman Jr., *J. Opt. Soc. Am.* **B2**, 1934 (1985)

[80] S. Blundell, P. Baird, C. Palmer, D. Stacey and G. Woodgate, *J. Phys.* **B20**, 3663 (1987)

[81] G. Torbohm, B. Fricke and A. Rosèn, *Phys. Rev.* **A31**, 2038 (1985)

[82] M. Crawford and A. Schawlow, *Phys. Rev.* **76**, 1310 (1949)

[83] C. Moore, *Atomic Energy Levels III*, National Standard Reference Data Series NSRDS-NBS, vol. **35**, National Bureau of Standards (U.S.) (1971)

[84] H. Rosenberg and H. Stroke, *Phys. Rev.* **A5**, 1992 (1972)

[85] S. Blundell, P. E. G. Baird, C. Palmer, D. Stacey, G. Woodgate and D. Zimmermann, *Z. Phys.* **A321**, 31 (1985)

[86] E. Fradkin, *Sov. Phys.* JETP **15**, 550 (1962)

[87] P. Aufmuth, *private communication* (1988,1990)

[88] C. Bernhardt, *Diplomarbeit*, Mainz (1990)

[89] P. Möller and J. R. Nix, Los Alamos Preprint LA-UR-86-3983 (1986)

[90] K. Kumar and M. Baranger, *Nucl. Phys.* **A122**, 273 (1968) and references therein

[91] U. Garg, A. Chaudhury, M. W. Drigert, E. G. Funk, J. H. Michelich, D. C. Radford, H. Helppi, R. Holzman, R. V. F. Janssens, T. L Khoo, and J. L. Wood, *Phys. Lett.* **180B**, 319 (1986)

[92] M. Finger, R. Foucher, J. P. Husson, I. Jastrzebski, A. Johnson, G. Astner, B. R. Erdal, A. Kjelberg, P. Patzelt, Å. Hoglund, S. G. Malmskog, R. Henck, *Nucl. Phys.* **A188**, 369 (1972)

[93] G. Hebbinghaus, T. Kutsarova, W. Gast, A. Kramer-Flecken, R. M. Lieder and W. Urban, *Nucl. Phys.* **A514**, 225 (1990)

[94] M. Piiparinen, J. C. Cunnane, P. J. Daly, C. L. Dors, F. M. Bernthal and T. L. Khoo, *Phys. Rev. Lett.* **34**, 1110 (1975)

Appendix 1

Derivation of the electric field gradient: The only stable platinum isotope with hyperfine structure (^{195}Pt) has a nuclear spin I = 1/2. Hence no information exists from stable isotopes on spectroscopic quadrupole moments and electric field gradients. In order to derive Q_s of the unstable isotopes from the measured B-factor in the $5d^9 6s\,^3D_3$ ground state, the electric field gradient has to be calculated. In case of the Pt ground state this gradient is related to the $5d_{5/2}$-hole by [78]

$$\langle \varphi_{JJ}(0) \rangle = - \frac{e}{4\pi\varepsilon_o} \frac{2j-1}{2j+1} \langle r^{-3} \rangle R_r(l, j, Z_i) \qquad (A.1)$$

R_r is a relativistic correction tabulated in [78] with the effective charge $Z_i = Z - 11$. For a d-hole, $R_r(l=2, j=5/2, Z_i=67) = 1.0833$. The expectation value $\langle r^{-3} \rangle$ can be calculated from the fine structure splitting $\delta\tilde{W}(^3D_1 - ^3D_3) = 10131.887\ cm^{-1}$ [79] with a relativistic correction $H_r(l=2, Z_i=67) = 1.0328$ tabulated in [78]. The results are

$$\langle r^{-3} \rangle = 67.63\ \text{Å}^{-3} \qquad (A.2)$$

$$\langle \varphi_{JJ}(0) \rangle = 6.79 \cdot 10^{22}\ V/m^2 \qquad (A.3)$$

and yield

$$B(^3D_3) = - 1.46\ GHz/b \cdot Q_s \qquad (A.4)$$

by use of (4).

Appendix 2

Derivation of the electronic factor F_{266}: The electronic factor F_i is required in order to calculate via (12) the changes of the nuclear charge radii from the field shift extracted out of the measured isotope shifts in the λ = 266 nm transition. The electronic factor F_{266} is proportional to the change of the relativistic electron density at the site of the nucleus during the optical transition. It is given by [80,81]

$$F_i = \frac{2\pi}{3} Z \alpha \hbar c\, \Delta|\Psi(0)|^2 = 3.916 \cdot 10^{-4} \cdot 4\pi Z a_0^3\, \Delta|\Psi(0)|^2\ GHz/fm^2. \qquad (A.5)$$

A multi-configuration Dirac Fock (MCDF) calculation yields for the $5d^9 6s\,^3D_3$ - $5d^9 6p\ 7_4$, λ = 266 nm transition a change of the relativistic electron density at the site of the nucleus of [35]

$$4\pi\, \Delta|\Psi(0)|^2 = 680.4\ a_0^{-3}\ . \qquad (A.6)$$

This results into an electronic factor of

$$F_{266}(MCDF) = -20.78\ GHz/fm^2\ . \qquad (A.7)$$

Another possibility to calculate F_{266} is to derive the non-relativistic electron density of the 6s electron at the site of the nucleus by the Fermi-Goudsmit-Segrè formula [78,82] from the fine structure energies or from the measured magnetic hyperfine structure by a calculation of the magnetic hyperfine field produced by the 6s electron at the nucleus [78].

$|\Psi(0)|^2$ derived according to the Fermi-Goudsmit-Segrè formula: The electron density at the nucleus is given by

$$|\Psi(0)|^2 = \frac{Z}{\pi a_0^3 n_a^3} \left(1 - \frac{d\sigma}{dn}\right) \qquad (A.8)$$

with the effective main quantum number $n_a = n - \sigma$ and the quantum defect σ. With $1 - d\sigma/dn = 1.347$ [83] the 6s electron density is given by

$$|\Psi(0)|^2_{6s} = 17.9\ a_0^{-3} \quad . \qquad (A.9)$$

$|\Psi(0)|^2$ from the hyperfine structure: The 6s electron density is related to the A-factor in the ^{195}Pt ground state by

$$|\Psi(0)|^2_{6s} = A(5d^9\ 6s) \cdot \left(\frac{8\pi}{3} h c R \alpha^2 a_0^3 F_r(j,Z)(1-\delta)(1-\varepsilon) \frac{\mu_I}{I\mu_B}\right)^{-1}. \qquad (A.10)$$

With $A(^{195}Pt) = 5.702647(23)$ GHz, $\mu_I(^{195}Pt) = 0.60949(6)\,\mu_N$ [23,24], the relativistic correction $F_r(j=1/2, Z=78) = 2.141$ [78], the corrections for the finite size of the nucleus $\varepsilon = 0.025$ [78] and $\delta = 0.09$ [84] the electron density is determined to be

$$|\Psi(0)|^2_{6s} = 16.1\ a_0^{-3}. \qquad (A.11)$$

The average value of (A.9) and (A.11)

$$|\Psi(0)|^2_{6s} = 17.0\ a_0^{-3} \qquad (A.12)$$

will be used in the following.
The electronic factor F_{266} is related to the change of the electron densities in the $\lambda = 266$ nm transition by

$$F_{266} = f(Z) \cdot E_{266} \qquad (A.13)$$

and

$$E_{266} = -\frac{\pi}{Z} a_0^3\ \Delta|\Psi(0)|^2_{6s \rightarrow 6p} \cdot \qquad (A.14)$$

$f(Z) = 60.23$ GHz/fm^2 is a relativistic correction [85]. The change of the electron densities in the transition can be traced back to the electron density in the 6s ground state by a screening factor [81]

$$\Delta|\Psi(0)|^2_{6s \rightarrow 6p} = \beta\,|\Psi(0)|^2_{6s} - |\Psi(0)|^2_{6p} \quad . \qquad (A.15)$$

The contribution $|\Psi(0)|^2_{6p}$ of the p electron to the transition density can be determined according to [86] by

$$\delta T_{6p_{1/2}} / \delta T_{6s} = \alpha Z/(1+\sigma) \quad , \quad \sigma = \sqrt{1 - (\alpha Z)^2} \tag{A.16}$$

to be 10 %. Hence, eq. (A.15) reduces to

$$\Delta|\Psi(0)|^2 = \beta \cdot 0.9 \, \Delta|\Psi(0)|^2_{6s} \quad . \tag{A.17}$$

The electronic screening factor has been calculated by Aufmuth [87] to be $\beta = 1.14$ under the assumption of pure Russel-Saunders coupling and the assignment of the 7_4 state as a pure $^3F_4$ state. This results in an electronic factor

$$F_{266}^{FS+HFS} = -42.45 \text{ GHz/fm}^2 \tag{A.18}$$

by use of (A.12), (A.13), (A.14) and (A.17). This value is a factor two larger than the MCDF result. Generally, the MCDF and semi-empirical values differ by 10 % to maximum 30 % [81]. The strong deviation in case of platinum indicates, that the assumption of a pure $^3F_4$ excited state is not justified. If only the term shift of the $^3D_3$ ground state of $T(5d^9\ 6s) = 70(8)$ mK [33] is considered and analyzed with $|\Psi(0)|^2$ from the A-factor, the electronic factor of the $^3D_3$ term shift is determined to

$$F_{6s} = -39.60 \text{ GHz/fm}^2 \tag{A.19}$$

and $\lambda^{194,196} = 0.053(6)$ fm^2. If this parameter is used to derive F_{266} from the measured isotope shift, one obtains

$$F_{266} = -27.6 \text{ GHz/fm}^2. \tag{A.20}$$

The comparison with (A.7) yields a screening factor of $\beta = 0.7$. Such a screening can be explained by an admixture of only 8 % of the $5d^8\ 6s6p$ configuration to the $5d^9\ 6p$ (J=4) state [87]. As a consequence of this not completely clear situation and in order to be consistent with the analysis of the neighbouring isotopic chains of gold [10,11] and mercury [7], the MCDF value (14) is used. This value is also supported by the (preliminary) results of recent muonic experiments on stable Pt isotopes which are in agreement with the MCDF value [88].

Table 1: Isotope shifts in the λ = 266 nm transition, nuclear parameter λ and changes in the charge radii of platinum isotopes with mass number A and nuclear half life $T_{1/2}$. The nucleus ^{194}Pt is taken as reference isotope. Columns 3-5 give our results. The isotope shift determined by Duong et al. [13] are given in column 6. The half-lifes given in column 2 are substituted by the natural abundances for the stable isotopes.

A	$T_{1/2}$	$\delta\nu_{exp}^{194,A}$ [GHz]	$\lambda_{exp}^{194,A}$ [fm^2]	$\delta < r^2 >^{194,A}$ [fm^2]	$\delta\nu_{exp}^{194,A}$ [GHz] Ref. [13]
198	7.2%	−2.94(9)	0.145(7)	0.154(8)	−2.97(6)
196	25.3%	−1.42(4)	0.070(3)	0.074(4)	−1.42(7)
195	33.8%	−0.67(6)	0.033(4)	0.035(4)	−0.92(9)
194	32.9%	0.00	0.000	0.000	0.00
193	50.0 y	0.89(11)	−0.044(6)	−0.047(7)	—
192	0.79%	1.28(17)	−0.064(10)	−0.067(10)	1.23(8)
191	2.9 d	2.65(11)	−0.131(7)	−0.139(8)	2.68(9)
190	0.01%	2.53(10)	−0.126(8)	−0.132(8)	2.44(7)
189	10.9 h	3.45(17)	−0.171(12)	−0.181(13)	3.50(9)
188	10.2 d	3.62(6)	−0.181(7)	−0.190(8)	3.52(7)
187	2.35 h	3.35(28)	−0.169(19)	−0.175(20)	3.47(7)
186	2.0 h	3.88(10)	−0.195(11)	−0.203(12)	3.97(10)
185g	70.9 m	—	—	—	1.53(12)
185m	33.0 m	3.69(27)	−0.187(20)	−0.193(21)	—
184	17.3 m	4.42(35)	−0.223(24)	−0.232(26)	—
183	6.6 m	3.17(68)	−0.164(41)	−0.166(45)	—

Table 2: Hyperfine structure constants of the $^3D_3$ ground state and 7_4 excited state for the odd platinum isotopes. The A-factor of the 7_4 excited state is determined by the ratio $A(^3D_3)/A(7_4)$= 3.78(1) of the stable isotope ^{195}Pt. The A-factor of the ground state for ^{195}Pt is from Ref. [23].

A	I	$A(^3D_3)$ [GHz]	$B(^3D_3)$ [GHz]	$B(7_4)$ [GHz]
195	$^1/_2$	+5.702647(23)	—	—
193	$^1/_2$	+5.64(5)	—	—
191	$^3/_2$	−1.54(2)	+1.26(16)	+0.42(13)
189	$^3/_2$	−1.37(2)	+1.77(31)	+0.34(17)
187	$^3/_2$	−1.33(6)	+1.61(11)	+0.33(14)
185m	$^1/_2$	+5.05(7)	—	—
183	$^1/_2$	+4.87(25)	—	—

Table 3: Spins and magnetic moments of odd-A platinum isotopes. The magnetic moments μ_I are calculated by use of (7) taking a correction for diamagnetism into account. Data obtained by nuclear orientation [25-27] and laser spectroscopy [13] are given for comparison.

A	I	μ (μ_N) this work	μ (μ_N) Ref. [13]	$\|\mu\|$ (μ_N) Ref. [25,26]	$\|\mu\|$ (μ_N) Ref. [27]
195	$^1/_2$	+0.60949(6)	—	—	—
193	$^1/_2$	+0.603(8)	—	—	—
191	$^3/_2$	−0.494(8)	−0.501(5)	0.500(10)	0.492(10)
189	$^3/_2$	−0.440(8)	−0.421(5)	0.434(9)	0.427(9)
187	$^3/_2$	−0.427(20)	−0.397(5)	0.408(8)	—
185g	$^9/_2$	—	−0.83(1)	0.774(14)	—
185m	$^1/_2$	+0.540(9)	—	—	—
183	$^1/_2$	+0.521(27)	—	—	—

Table 4: Spectroscopic quadrupole moments of odd-A platinum isotopes deduced from the B($^3D_3$)-factors (Table 2) by means of equation (8). Data obtained by laser spectroscopy [13] and nuclear orientation [25,26] are given for comparison. For Q_s^{corr} a Sternheimer antishielding factor of R = -0.1 is applied to the weighted mean of the two laser measurements.

A	Q_S [b] this work	Q_S [b] Ref. [13]	Q_S [b] Ref. [25,26]	Q_S^{corr} [b]
191	−0.86(11)	−0.98(5)	−0.64(26)	−0.87(4)
189	−1.21(21)	−1.03(5)	−0.65(26)	−0.95(4)
187	−1.10(8)	−1.13(5)	−0.85(39)	−1.02(4)
185g	—	+4.3(5)	+2.1(9)	+3.91(45)

Table 5: Results of a multi-dimensional King plot analysis. All data on isotope shifts in several optical transitions are taken into account. This data set is used for further analysis of the isotope shift.

A	$\delta\nu_{exp}^{194,A}$ [GHz]	$\lambda^{194,A}$ [fm^2]	$\delta < r^2 >^{194,A}$ [fm^2]
198	−2.889(48)	0.143(5)	0.151(6)
196	−1.413(29)	0.070(3)	0.074(4)
195	−0.675(43)	0.033(3)	0.035(3)
194	0.000	0.000	0.000
193	0.89(11)	−0.044(6)	−0.047(7)
192	1.372(30)	−0.068(3)	−0.072(3)
191	2.671(74)	−0.132(6)	−0.140(6)
190	2.561(40)	−0.127(5)	−0.134(5)
189	3.508(92)	−0.174(8)	−0.184(9)
188	3.589(52)	−0.179(7)	−0.188(7)
187	3.485(86)	−0.175(9)	−0.183(10)
186	3.942(79)	−0.198(10)	−0.207(11)
185g	1.53(12)	−0.083(12)	−0.080(14)
185m	3.69(27)	−0.187(20)	−0.193(21)
184	4.42(35)	−0.223(24)	−0.232(26)
183	3.17(68)	−0.164(41)	−0.166(45)

Table 6: Model-dependent quadrupole deformation parameters $\delta\langle\beta^2\rangle^{194,A}$ and $\langle\beta^2\rangle^{1/2}$ as calculated by use of (16) and (18) from the isotope shifts (last column of Table 5). The B(E2)-value of ^{194}Pt [46] served for calculating the absolute deformation parameters. The known B(E2)-values for the even-even Pt isotopes [47] are given for comparison. The last column shows the deformation parameters as calculated from the spectroscopic quadrupole moments after converting them into intrinsic ones under the assumption of strong coupling for hypothetical axially symmetric nuclei.

A	$\delta < \beta_2^2 >^{194,A}$	$\lvert < \beta_2^2 >^{1/2} \rvert$	$\lvert < \beta_2^2 >^{1/2} \rvert$ (B(E2))	$< \beta_2 >$ (Q_s)
198	−0.0050(7)	0.12(1)	0.1130(27)	—
196	−0.0027(3)	0.13(1)	0.1308(19)	—
195	−0.0015(3)	0.14(1)	—	—
194	0.0000	0.1434(26)	0.1434(26)	—
193	0.0005(6)	0.14(1)	—	—
192	0.0033(9)	0.15(1)	0.1549(24)	—
191	0.0017(7)	0.15(1)	—	−0.15(2)
190	0.0068(7)	0.16(1)	0.149(9)	—
189	0.0071(11)	0.17(1)	—	−0.21(4)
188	0.0109(7)	0.18(1)	0.183(17)	—
187	0.0166(17)	0.19(1)	—	−0.19(2)
186	0.0188(10)	0.20(1)	0.1976(38)	—
185m	0.0238(18)	0.21(1)	—	—
184	0.0250(22)	0.21(1)	0.2292(40)	—
183	0.0350(38)	0.24(1)	—	—

Table 7: Particle-triaxial rotor model calculation parameters ε_2 and γ (see Section 4) and the mean field TRS calculation parameters β_2, β_4, and γ (see Section 5).

A	N	π	ε_2	γ [deg]	β_2	β_4	γ [deg]
195	117	-	0.120	52.0			
193	115	-	0.150	35.0	0.15	-0.028	52
		+	0.168	31.0	0.14	-0.025	66
191	113	-	0.150	31.7	0.15	-0.030	36
		+	0.168	33.0	0.15	-0.027	47
189	111	-	0.155	32.0	0.17	-0.029	26
		+	0.176	32.0	0.15	-0.024	43
187	109	-	0.169	30.0	0.20	-0.046	10
		+	0.180	28.5	0.19	-0.041	13
185	107	-	0.227	23.0	0.22	-0.036	10
		+	0.230	22.0	0.22	-0.036	1
183	105	-	0.240	20.0	0.24	-0.023	0
		+	0.230	21.0	0.23	-0.025	0
181	103	-	0.240	16.0	0.26	-0.008	0
		+	0.240	17.5	0.24	-0.010	0
179	101	-			0.25	0.005	0
		+			0.26	0.004	0
177	99	-	0.207	17.0	0.25	0.016	0
		+	0.270	16.0	0.19	-0.005	14
					0.24	0.013	1

Table 8: Comparison of deformation parameters extracted from different experiments and model calculations. **a)** ε_2 values fitted in the present PTR calculation for ground states of $^{177-195}$Pt ($\gamma \neq 60^0$, see Table 7). **b)** ε_2 values calculated by Möller and Nix [89] for axially symmetrical shape and $\varepsilon_4 \neq 0$ and $\varepsilon_6 \neq 0$. **c)** β_2 values extracted by Bengtsson et al. [63] from experimental B(E2) values. To deduce $|\beta_2|$, for $^{176-188}$Pt prolate shape and B(E2, $8^+ \rightarrow 6^+$), for $^{190-196}$Pt oblate shape and B(E2, $2^+ \rightarrow 0^+$) were used. **d)** β_2 obtained as minima in the potential energy surfaces calculated with the Woods-Saxon potential. See Ref. [56] for details. **e)** Results of standard self-consistent HFB using Kumar-Baranger many-body wave function [89] calculated without hexadecapole deformation with $\gamma = 0^0$, 20.2^0 and 60^0 for A=186, 188 and 190-196 resectively. See Refs. [55] and [57] for details. **f)** β_2 values extracted from known $\delta\langle r^2\rangle$ using weighted least squares fit [14]. **g)** Experimental data taken from Refs. [65] (A=176,178), [66] (A=180), [91](A=184), [92] ($182 \leq A \leq 192$), [93](A=186), [94](186 ≤ A ≤ 194). Where not specified, current Nucl. Data Sheets were used.

A	ε_2 [a]	ε_2 [b]	$\lvert\beta_2\rvert$ [c]	$\lvert\beta_2\rvert$ [d]	$\lvert\beta_2\rvert$ [e]	$\lvert\langle\beta_2^2\rangle^{1/2}\rvert$ [f]	E_2^{exp} [g] [MeV]	E_2^{cal} [MeV]	E_4/E_2^{exp} [g]	E_4/E_2^{cal}
196		-0.131	0.13(1)	0.12	0.125	0.13(1)	0.356		2.46	
195	0.120	-0.144				0.14(1)				
194		-0.138	0.14(1)	0.13	0.134	0.1434(26)	0.328	0.327	2.47	2.90
193	0.150	-0.144				0.14(1)				
192		-0.144	0.16(1)	0.14	0.144	0.15(1)	0.292	0.272	2.48	2.84
191	0.150	-0.151				0.15(1)				
190		-0.151	0.17(2)	0.15	0.155	0.16(1)	0.296	0.315	2.49	2.67
189	0.155	0.151				0.17(1)				
188		0.158	0.17(2)	0.18	0.170	0.18(1)	0.266	0.301	2.53	2.70
187	0.169	0.192				0.19(1)				
186		0.192	0.18(1)	0.20	0.188	0.20(1)	0.192	0.263	2.56	2.66
185	0.230	0.212				0.23(1)				
184		0.205	0.23(2)	0.22		0.21(1)	0.163	0.129	2.67	3.00
183	0.240	0.225				0.24(1)				
182		0.212		0.23			0.155	0.116	2.71	3.11
181	0.240	0.235								
180		0.225		0.24			0.153	0.109	2.68	3.27
179		0.239								
178		0.171	0.22(1)	0.24			0.170		2.51	
177	0.270	0.232								
176		0.151	0.20(1)	0.22			0.264	0.093	2.14	3.22

Table 9: Electromagnetic moments of $^{177-193}$Pt . **a)** Present work. g_{eff} = 0.7; for model parameters see Table 7. **b)** Calculation of Duong et al. [13] using Nilsson model and g_{eff} = 0.6. **c-d)** Calculation of Duong et al. [13] using particle-axially symmetrical rotor model with single-particle wave functions from HFB calculation; g_{eff} = 0.6, the core nucleus is $^{A-1}$Pt for (c) and $^{A+1}$Pt for (d). For more details see Ref. [13]. **e)** Present work, $\gamma = 0^0$. **f)** Present work, $\gamma = 60^0$.

A	I^π	Q^{cal} [eb]	μ^{cal} [n.m.]	μ^{cal} [n.m.]	μ^{cal} [n.m.]	μ^{cal} [n.m.]
193	$1/2^-$		+0.51 +0.47 f)			
191	$3/2^-$	−0.74 −0.76 f)	−0.51 −0.31 f)	+0.39	+0.31	+0.19
189	$3/2^-$	−0.79 −0.80 f)	−0.44 −0.24 f)	+0.39	+0.39	+0.31
187	$3/2^-$	−0.97 −0.89 f)	−0.36 −0.13 f)	+0.39	+0.53	+0.39
185^m	$1/2^-$		+0.46 +0.47 e)			
185	$9/2^+$	+3.46 +3.93 e)	−0.93 −0.90 e)	−0.45	−0.73	−0.79
183^m	$7/2^-$	+3.35 +3.68 e)	+0.86 +0.91 e)			
183	$1/2^-$		+0.45 +0.47 e)			
181	$1/2^-$		+0.45 +0.47 e)			
177^m	$1/2^-$		+0.46 +0.47 e)			
177	$5/2^-$	+3.00	−0.31 −0.52 e)			

FIGURE CAPTIONS

Figure 1: Experimental set-up for on-line resonance ionization mass spectroscopy of radioactive platinum isotopes. Mercury ions which were produced and mass separated at the on-line mass separator ISOLDE-3 at CERN/Geneva are implanted with 60 keV into a target wheel made of graphite. After a delay adjusted to the decay time of the Hg mother isotope to the Pt daughter, the wheel was turned by 180^0 and a pulsed thermal atomic beam was formed by laser desorption. The atoms desorbed are analyzed by RIMS. The ion deflector in the TOF spectrometer shields the microchannel plate detector against radioactivity.

Figure 2: Part of the atomic level scheme of platinum. The excitation steps used in the RIMS/PLID-experiment are indicated.

Figure 3: Resonance signals of laser-desorbed ^{191}Pt (I = 3/2; upper part) and ^{183}Pt (I = 1/2, $T_{1/2}$ = 6.5 min; lower part) versus the laser frequency in the first excitation step as obtained by resonance ionization mass spectroscopy. The solid lines represent fits to the data points. In the case of ^{183}Pt, $3 \cdot 10^9$ ions of ^{183}Hg were implanted into the target wheel.

Figure 4: Mean-square charge radii of platinum, gold and mercury isotopes as function of mass number. The radii of ground states are indicated and connected by an eye-guiding line. In addition, the charge radii of isomeric states are given. The errors are smaller than the diameters of the symbols except for ^{183}Pt and ^{184}Au. In addition, there is a common scaling uncertainty for each isotopic chain of the order of 10 %. The $\langle r^2 \rangle$-values for platinum were calculated from the $\delta \langle r^2 \rangle$-values given in Table 5. For absolute $\langle r^2 \rangle$ -values, the mean-squared charge radius of ^{198}Pt was calculated by means of the Droplet model [42]. Quadrupole deformation was taken into account by use of the B(E2)-value of ^{194}Pt [46]. Similarly, the data for gold [10,11] and mercury [7] were derived with ^{197}Au and ^{204}Hg as reference nuclei.

Figure 5: Quadrupole deformation parameters $\langle \beta^2 \rangle^{1/2}$ of platinum, gold, and mercury isotopes as a function of mass number as calculated from the measured isotope shifts. The guiding line is connecting the ground states. In addition, the quadrupole deformation parameters of the isomeric states are given. The values for platinum are taken from Table 6, those for gold and mercury from Ref. [7,10,11].

Figure 6: Calculated magnetic moments (a), quadrupole moments (b) and energies of the lowest 3/2-states (c) in ^{187}Pt for ε_2 = 0.15, 0.169 and 0.22 as a function of γ-deformation (connected by eye-guiding lines). Experimental values of the quadrupole and magnetic moments are also given.

Figure 7: Total Routhian Surfaces for $^{175-193}$Pt. The surface displays configurations with negative parity and signature α = -1/2 at a rotational frequency of $\hbar\omega$ = 0.05 MeV. The energy difference between the contour lines is 100 keV. Note the smooth transition from prolate to oblate with increasing neutron number.

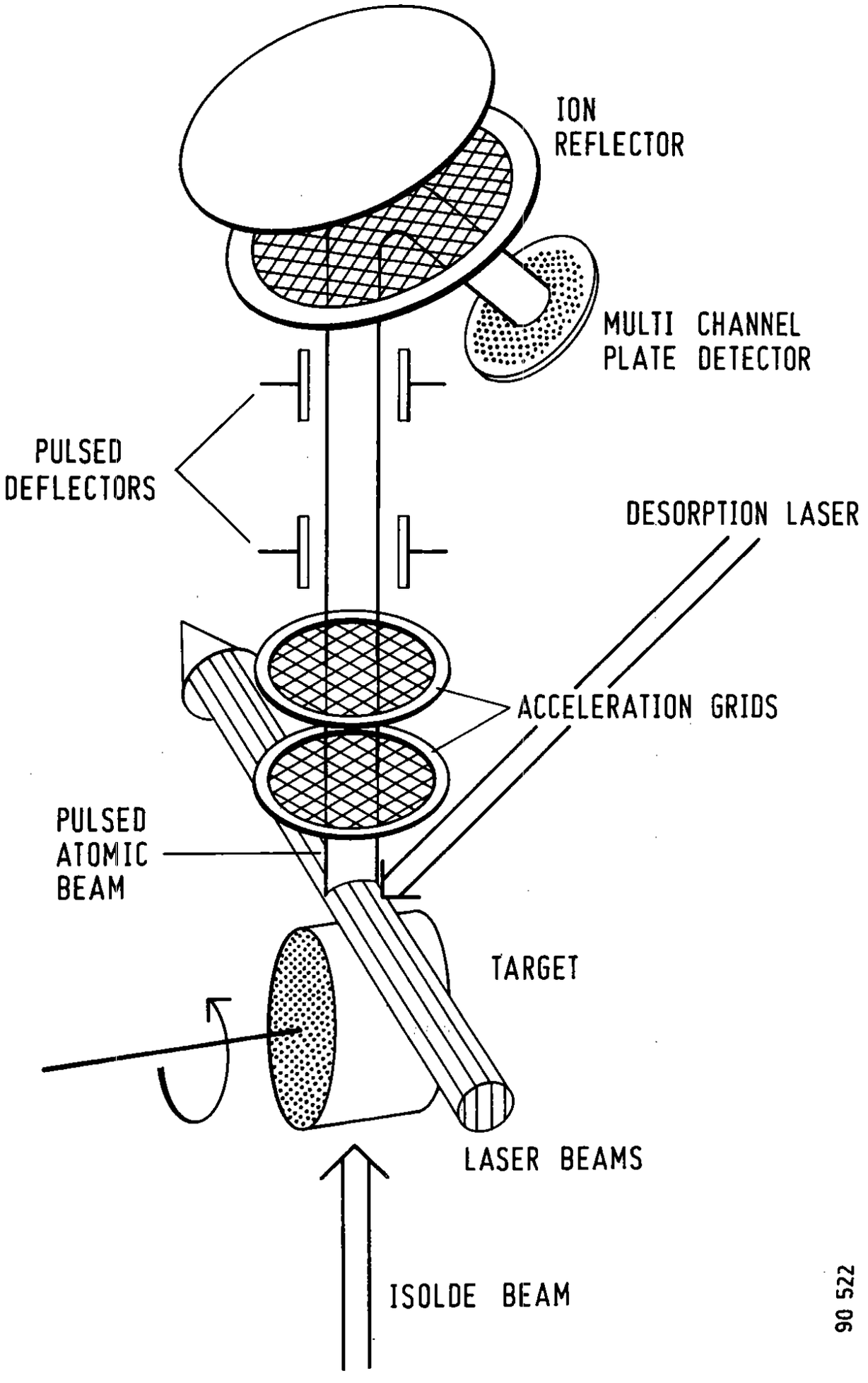
ION
REFLECTOR
MULTI CHANNEL
PLATE DETECTOR
PULSED
DEFLECTORS
DESORPTION LASER
ACCELERATION GRIDS
PULSED
ATOMIC
BEAM
TARGET
LASER BEAMS
ISOLDE BEAM
90 522

Fig. 1

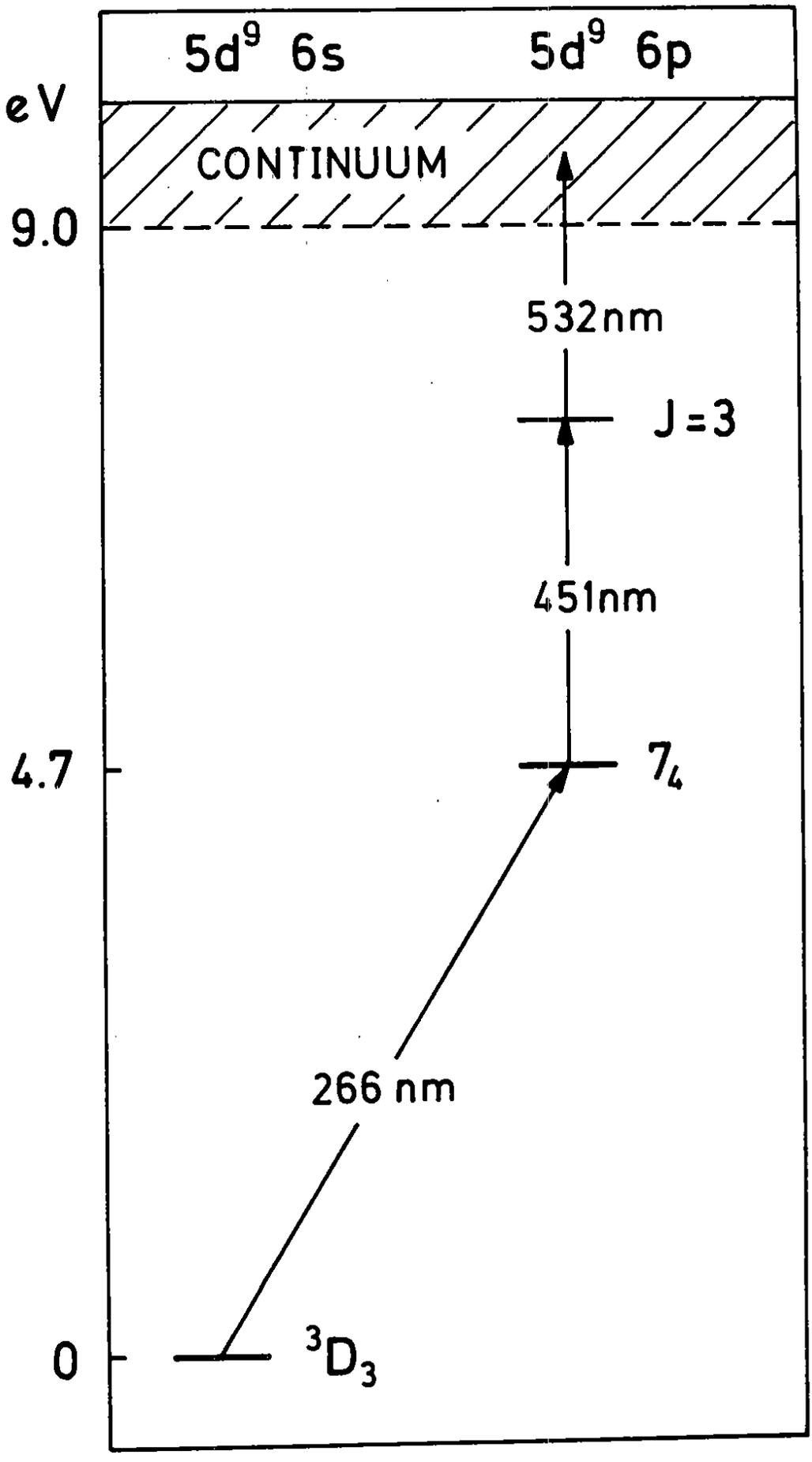

89 758

Fig. 2

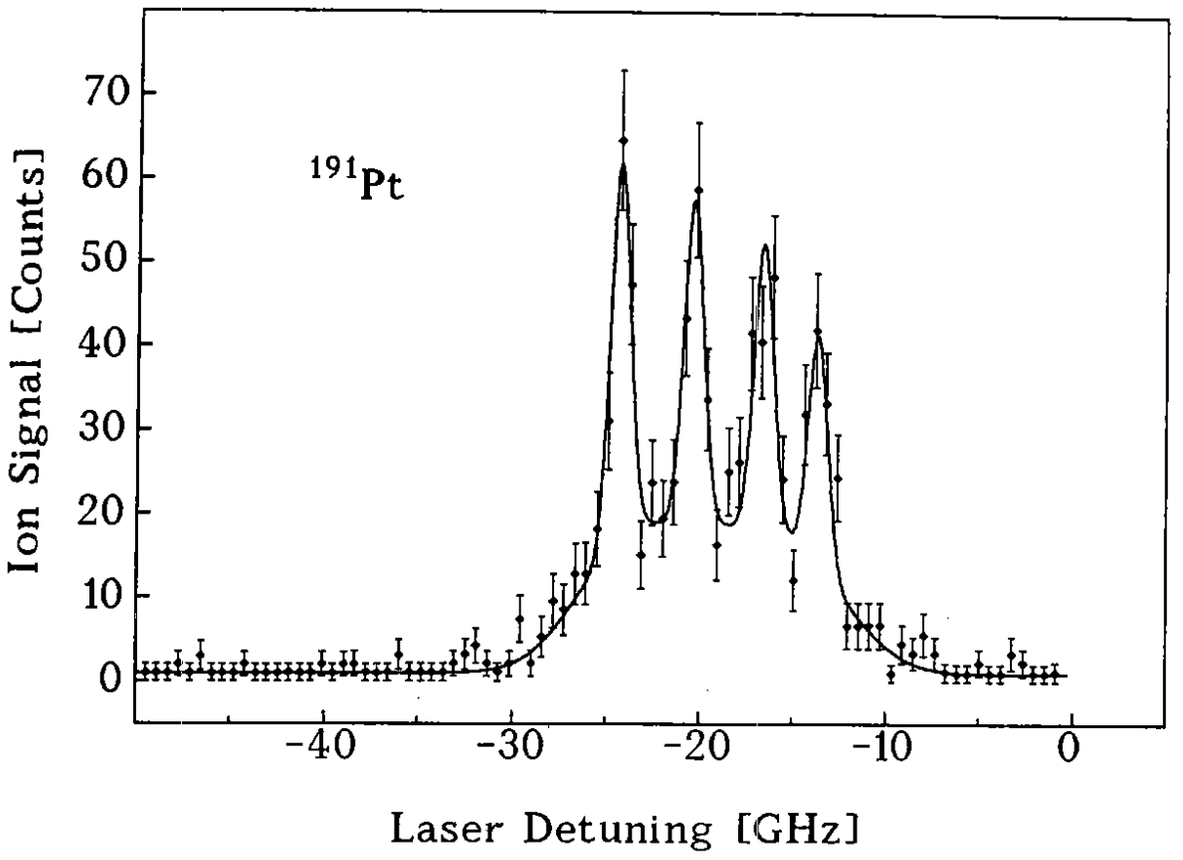
^{191}Pt
Ion Signal [Counts]
70
60
50
40
30
20
10
0
-40
-30
-20
-10
0
Laser Detuning [GHz]

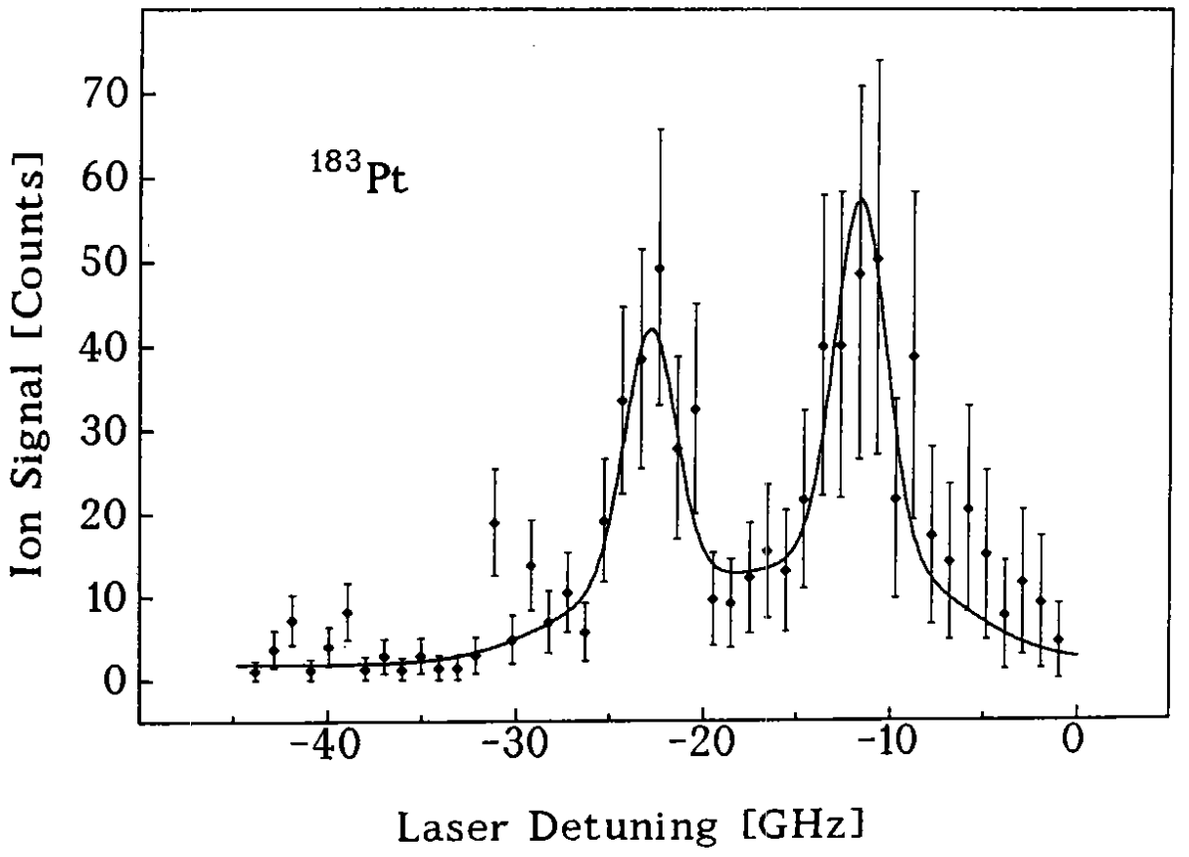
^{183}Pt
Ion Signal [Counts]
70
60
50
40
30
20
10
0
-40
-30
-20
-10
0
Laser Detuning [GHz]

91315

Fig. 3

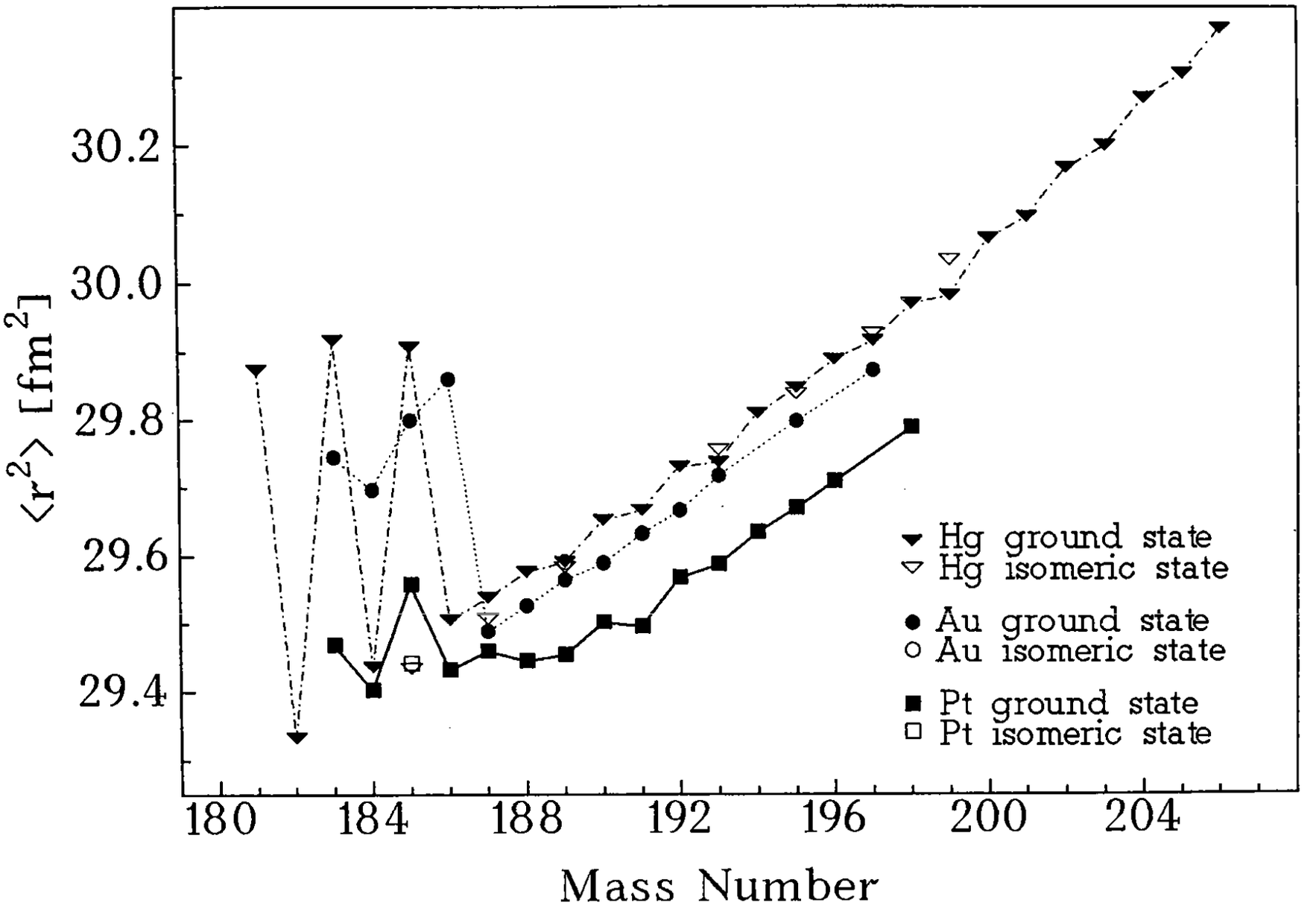
30.2
30.0
29.8
29.6
29.4
$\langle r^2 \rangle$ [fm^2]
180
184
188
192
196
200
204
Mass Number
Hg ground state
Hg isomeric state
Au ground state
Au isomeric state
Pt ground state
Pt isomeric state
91 313

Fig. 4

Hg ground state
Hg isomeric state
Au ground state
Au isomeric state
Pt ground state
Pt isomeric state
0.28
0.24
0.20
0.16
0.12
$\langle\beta^2\rangle^{1/2}$
180
184
188
192
196
200
204
Mass Number

Fig. 5

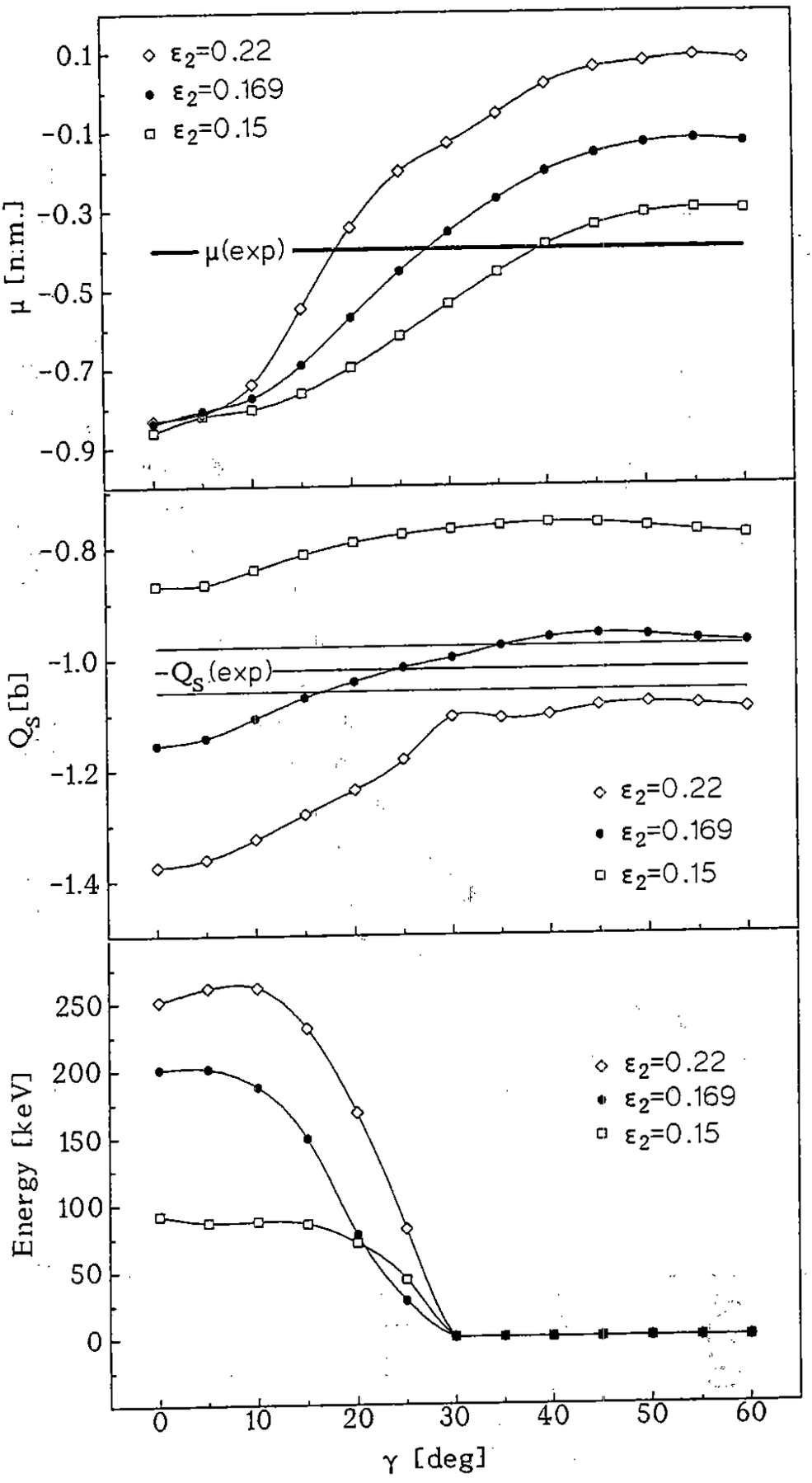
ε2=0.22
ε2=0.169
ε2=0.15
μ(exp)
μ [n.m.]
0.1
-0.1
-0.3
-0.5
-0.7
-0.9
-Qs(exp)
Qs [b]
-0.8
-1.0
-1.2
-1.4
Energy [keV]
250
200
150
100
50
0
0
10
20
30
40
50
60
γ [deg]

Fig. 6

Imprimé au CERN. Prix : 1.40 Fr.

Fig. 7